

# Harmonic QPOs and Thick Accretion Disk Oscillations in BL Lac Object AO 0235+164

F.K. Liu, G. Zhao

and

Xue-Bing Wu

fkliu@bac.pku.edu.cn, wuxb@bac.pku.edu.cn

*Astronomy Department, Peking University, 100871 Beijing, China*

## ABSTRACT

Periodic outbursts are observed in many AGNs and usually explained with a supermassive black hole binary (SMBHB) scenario. However, multiple periods are observed in some AGNs and cannot be explained with it. Here we analyze the periodicity of the radio light curves of AO 0235+164 at multi-frequencies and report the discovery of six QPOs in integer ratio 1:2:3:4:5:6 of QPO frequencies, of which the second with period  $P_2 = (5.46 \pm 0.47)$  yr is the strongest. We fit the radio light curves and show that the initial phases of six QPOs have zero or  $\pi$  differences relative to each other. We suggest a harmonic relationship of QPOs. The centroid frequency, relative strength, harmonic relationship and relative initial phases of QPOs are independent of radio frequency. The harmonic QPOs are likely due to the quasi-periodic injection of plasma from an oscillating accretion disk into the jet. We estimate the supermassive black hole mass  $M_{\text{BH}} \simeq (4.72 \pm 2.04) \times 10^8 M_{\odot}$  and the accretion rate  $\dot{m} \simeq 0.007$ . With the knowledge of accretion disk, it implies that the inner region of accretion disk of AO 0235+164 is a radiatively inefficient accretion flow. The oscillation accretion is due to the p-mode oscillation of the thick disk probably excited by a SMBHB. The theoretical predications of fundamental oscillation frequency and the harmonics are well consistent with the observations. Harmonic QPOs would be absent when the thick disk becomes geometrically thin due to the increase of accretion rate. We discuss the observations of AO 0235+164 basing on the SMBHB-thick disk oscillation scenario.

*Subject headings:* accretion, accretion disks — galaxies: active — BL Lacertae objects: individual (AO 0235+164) — galaxies: interactions — radio continuum: galaxies — hydrodynamics

## 1. Introduction

Blazars, consisting of BL Lac objects and flat-spectrum radio quasars, are a subclass of AGNs whose relativistic jet is nearly aligned to the line of sight, and show extreme variabilities at from radio through optical and X-ray to high-energy  $\gamma$ -ray wavelengths (Antonucci 1993; Urry & Padovani 1995; Wagner & Witzel 1995; Ulrich et al. 1997). Long term multi-wavelength monitorings show that the variabilities of blazars are very complex with large amplitude and on time-scale ranging from tens of minutes, hours and days to months and years at all wavelengths. The outbursts with time-scale of order of years or longer in some blazars are periodic (Sillanpää et al. 1988; Liu et al. 1995a, 1997; Raiteri et al. 2001; Qian & Tao 2004) and of particular interest as it might connect to the presence of supermassive black hole binary (SMBHB) at center (Sillanpää et al. 1988; Liu & Wu 2002; Qian & Tao 2004; Ostorero et al. 2004), whose ultimate coalescence would generate an outburst of gravitational wave radiation (Thorne & Braginskii 1976) and be the main target of a future space gravitational wave detector, Laser Interferometer Space Antenna (LISA) (Merritt et al. 2005).

SMBHBs in galactic nuclei are expected by the hierarchical galaxy formation model in the cold dark matter (CDM) cosmology (Kauffmann & Haehnelt 2000) in which the present galaxies are the products of frequent galaxy minor mergers. Active SMBHB and final coalescence have been suggested to be the physical origin of the peculiar radio morphologies in some AGNs (for a recent review, see Komossa 2003), e.g. the helical morphology of radio jets (Begelman et al., 1980), the interruption and recurrence of activity in double-double radio galaxies (Liu, Wu & Cao 2003), the X-shaped feature of winged radio sources (Merritt & Ekers 2002; Liu 2004), the orbital motion of radio core (e.g. Sudou et al. 2003). Since they were discovered in BL Lac object OJ287 (Sillanpää et al. 1988), periodic optical outbursts of blazars have been ascribed to the orbital motion of SMBHB (Sillanpää et al. 1988; Abraham & Romero 1999; Valtaoja et al. 2000; Liu & Wu 2002; Rieger 2004; Lobanov & Roland 2005). However, it is unclear how SMBHBs in AGNs trigger the observed periodic outbursts if present. The proposed scenarios in literature include (1) direct impact of the secondary black hole against a standard thin accretion disk (e.g. Lehto & Valtonen 1996)) or an inefficient accretion flow, e.g. advection dominated accretion flow

(ADAF; Liu & Wu 2002), (2) rotating helical jets due to the orbital motion of SMBHB (Katz 1997; Villata et al., 1998; Ostorero et al. 2004; Rieger 2004), (3) periodic change of jet orientation introduced by the Lens-Thirring precessing of a warped disk (Abraham & Romero 1999; Lobanov & Roland 2005). Although the detailed physical mechanisms in these models are different, all of them suggest a common feature of single period in the light curves.

One more complication to the investigation of the periodicity in blazars is from the observations of low frequency X-ray quasi-periodic oscillations (QPOs) in black hole X-ray binaries (Hasinger et al. 1986; van der Klis 1989; Strohmayer et al. 1996) and possibly in Sgr A\* of our Galactic center (Török 2005), which are believed to be due to the disk oscillations. Black hole X-ray binaries, so called micro-quasars, are physical analogue to AGNs and are powered by accretion of stellar black holes of mass about  $10M_{\odot}$ . As the variation time-scale of accretion disk around black holes is proportional to the mass of black hole and the formation of jet is coupled with accretion disk (Gallo et al. 2003; Fender & Belloni 2004; Fender et al. 2004), the low frequency QPO with typical frequency  $\sim 1\text{Hz}$  in micro-quasars corresponds to a period of order of years or longer in a blazar system of black hole mass larger than  $10^8M_{\odot}$ . Disk oscillations may cause a periodic change of accretion and the QPOs in X-ray black hole binary system (Rezzolla et al. 2003a), which could lead to periodic jet emission due to the jet-disk coupling.

To understand the physical origin of periodic outbursts, it is essential to investigate in details the structure of periodic outbursts in both light curves and power density spectrum, and the dependence of periodicity on the observational wavelengths. For example, the discovery of double peaks in the periodic optical outbursts of the BL Lac object OJ287 (Sillanpää et al. 1996) leads to the second version of the SMBHB model (Lehto & Valtonen 1996), while the investigation of the relation of the optical outburst structure and the radio variations leads to the third version of the SMBHB scenario (Valtaoja et al. 2000; Liu & Wu 2002). It is generally believed that the short-term variabilities of blazars are non-periodic (e.g. Wagner & Witzel 1995; Ulrich et al. 1997), but the short-term periodic brightness flickering may have been found to superpose on the long-term periodic variations in some blazars, e.g. OJ287 (Wu et al., 2006) and 3C66A (Lainela et al. 1999). In order to give more constraints on the models for periodic outbursts in AGNs, recently we started a program to investigate the relationships of periodic major outbursts and minor events and the long- and short-term periodicities of a large sample of AGNs (Zhao, Liu, & Wu 2006). Here we report the results of multiple quasi-periodic oscillations (QPOs) and the harmonic resonant relationship 1:2:3:... of QPO frequencies in BL Lac object AO 0235+164.

BL Lac object AO 0235+164 with redshift  $z = 0.94$  is one of the most violently variable

object whose periodicity of outbursts in optical and radio bands has been investigated and reported in literature (e.g. Webb & Smith 1989; Webb et al. 2000; Roy et al. 2000; Raiteri et al. 2001, 2005). Roy et al. (2000) analyzed the data of the University of Michigan Radio Astronomy Observatory (UMRAO) at frequencies 4.8, 8.0 and 14.5 GHz from 1975 to 1999 and discovered a period  $\sim 5.8$  yrs at 8.0 and 14.5 GHz, which is consistent with the observations of a period 5.7 yrs in the optical (Raiteri et al. 2001, 2005). Ostorero et al. (2004) interpreted the long term periodicity of major outbursts with a helical-jet model and the minor events with rotation of the non-periodic inhomogeneity. However, the radio outbursts are double-peaked and the burst peaks do not appear as regularly as the period predicted (Raiteri et al. 2001, 2005), implying that the substructure of the outburst are complex. On the other hand, the multiple short periods though at much lower significant level of signal-to-noise and the poor identification of central frequency have been claimed in literature. Webb & Smith (1989) first identified the three peaks with three periods  $\sim 2.79$  yrs,  $\sim 1.58$  yrs, and  $\sim 1.29$  yrs in the Fourier power spectrum of the optical light curves. Subsequent observations marginally confirmed the periods with 2.7 and 1.2 years in optical (Webb et al. 2000) and with 1.8, 2.8 and 3.7 years in radio wave-bands with the Discrete Correlation Function (DCF) analysis method (Raiteri et al. 2001).

Our work is based on the three radio databases of the University of Michigan Radio Astronomy Observatory (UMRAO), the National Radio Astronomy Observatory (NRAO), and the Metsähovi Observatory. In Sec. 2, we start the investigations from analyzing the consistency of UMRAO’s and NRAO’s databases, by comparing the best-sampled observations at 8.0 GHz at UMRAO and those at 8.2 GHz at NRAO and then merging the observational data at these two frequencies. The periodic analysis results for the combined light curves at 8 GHz and identification of harmonic QPOs are given in Sec. 3. In Sec. 4, we investigate the dependence of QPO properties on radio frequency. After estimating the mass of central supermassive black hole (SMBH) and the accretion rate in Sec. 5.1, we analytically discuss the p-mode oscillation of thick disk in Sec. 5.2. A SMBHB-disk oscillation scenario for multiple harmonic QPOs is suggested and discussed in Sec. 6. Our discussions and conclusions are given in Sec. 7. We assume a flat cosmology with  $H_0 = 75 \text{ Km s}^{-1} \text{ Mpc}^{-1}$ ,  $\Lambda = 0$ , and  $q_0 = 0.5$  throughout the paper, leading to a source distance  $d \simeq 4.4 \text{ Gpc}$ .

## 2. Databases and the consistency

UMRAO has been monitoring AO 0235+164 at 4.8, 8.0, and 14.5 GHz for about three decades (Aller et al. 1985, 1999), while NRAO’s database contains the observational data at 2.5 and 8.2 GHz for about 20 years (Fiedler et al. 1987; Waltman et al. 1991; Lazio

et al. 2001). At frequencies 22 and 37 GHz, the Metsähovi Observatory started collecting the flux data since 1980 (Teräsraanta et al. 1998, 2004). As the central frequencies of 8.0 GHz and 8.2 GHz are almost the same and light curves at the two frequencies are best sampled in both databases of UMRAO and of NRAO, we investigate the consistence of the observations and construct a combined light curves, based on the data from both databases. The observations at UMRAO last about  $\sim 25$  years with a relatively sparse data sampling ( $\sim 0.1$  data points per day), while those at NRAO cover a shorter time of about 15 years with relatively dense data sampling ( $\sim 0.5$  data points per day). To remove the effects of intra-day variabilities (Romero et al. 1997) and of the noises due to unevenly sampling, we compose two quasi-simultaneous observational light curves by averaging the observational data with a 10-days time-interval, which is much shorter than the variability time-scale (of order of months) of major outbursts but give, respectively, about one and five observations in each bin at 8.0 GHz and 8.2 GHz to smooth the intra-day random variations.

The results are shown in Fig. 1. The standard error in Fig. 1 is the statistical error. A least square fit with a correlation coefficient  $r = 0.989$  gives

$$F_{8.0} = (-0.017 \pm 0.014) + (1.072 \pm 0.006)F_{8.2}, \quad (1)$$

where  $F_{8.0}$  and  $F_{8.2}$  are the radio flux at 8.0 GHz (UMRAO) and at 8.2 GHz (NRAO), respectively. The results show that the observations of UMRAO and of NRAO are consistent with each other with a linear relation but the slope is not exact unity. So we merged the observational data at 8.0 GHz and at 8.2 GHz and obtain a combined light curve by converting NRAO's observations with the fitted relations Eq. (1). The combined radio light curve at 8 GHz is given in Fig. 7, which shows that the combined light curves fully covers several major outbursts in details although the combined data do not cover a significant longer time. In the following sections, we will give the periodic analysis results and discussions, based on the combined light curve at 8 GHz. In order to show how efficient and to what extent the combination of two databases can improve the results, we also analyze the radio light curves at 8.0 GHz and 8.2 GHz, respectively.

### 3. Multiple QPOs in the combined 8 GHz light curve

We analyze the periodicity of the combined light curve at 8 GHz by computing the Fourier power spectrum with a Lomb normalized periodogram (Lomb 1976; Scargle 1982), which is designed to properly treat the unevenly sampled data. The power spectrum is showed in Fig. 2. There are several very prominent peaks in the power spectrum with very high signal-to-noise ratios. We identify a peak with a QPO if (1) it is at least 5 times higher

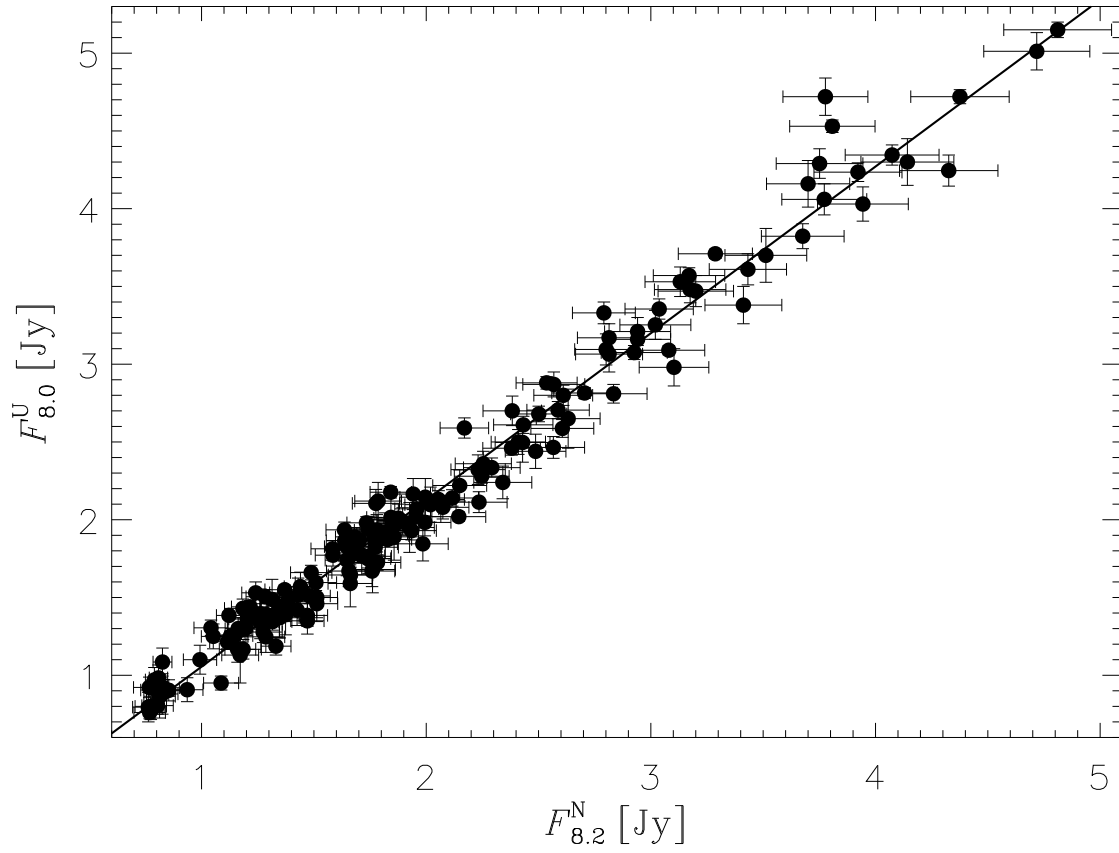


Fig. 1.— Correlations of the observations of UMRAO at 8.0 GHz (y-axis) and of NRAO at 8.2 GHz (x-axis). The data are 10-days averaged and the solid line is a least square fit.

than the nearby background noise; (2) it has a Gaussian profiles; (3) it is also detected with other periodic analysis methods, e.g. the Jurkevich  $V_m^2$  method (Jurkevich 1971) and the z-transform discrete correlation function (ZDCF) technique (Alexander 1997); and/or (4) it correlates with other QPOs, e.g. with a harmonic relationship.

Before discussing the periodic analysis results of the combined light curve, we firstly investigate the effects of the combination of the two databases. We analyze, respectively, with the Lomb method the light curves at 8.0 GHz at UMRAO and at 8.2 GHz at NRAO, and give the power spectra in Fig. 3. Fig. 2 and Fig. 3 show that all the peaks in Fig. 3 are present in Fig. 2 and the combination of two databases significantly improves the signal-to-noise ratio of the power spectrum, which of the combined light curve is unprecedentedly high. This is because the radio light curve at 8.0 GHz has relatively sparse data points and misses the structure information of the major bursts, while the observations at 8.2 GHz span a shorter observational time interval and give only broad peaks in the power spectrum with small coherent quality factors. The second effect one can read from Fig. 2 and Fig. 3 is that though most of the peaks in the power spectrum of the combined radio light curve can be found in the power spectra of the radio light curve at 8.0 GHz and 8.2 GHz, the central frequency of each peak is significantly different. A prominent peak of 8.50 years at the periodogram of radio light curve at 8.0 GHz is absent both at the power spectra of the combined radio light curve and of the light curve at 8.2 GHz. Therefore, it is probably spurious because of the low signal-to-noise ratio due to the incomplete coverage of major outbursts in the sparsely-sampled light curve at 8.0 GHz and to the loss of the burst structure information. To solve the problem, much more intensive observations are need.

The peaks in Fig. 2 are Gaussian, though some of them overlap with each other. Therefore, we fit each peak profile with a Gaussian function or, if necessary, fit several peak profiles together with Gaussian functions. The fitting results are given in Table 1. In Table 1, Col. 1 gives the observational radio frequency  $\nu_{\text{obs}}$ , the averaged period of the fundamental QPO and their standard errors. We will discuss the definition of fundamental QPO and how to calculate the average period later. The centroid frequency  $\nu$  and the standard error  $\sigma$  of each peak are given in Col. 2 and indicated in Fig. 2. The fitting goodness  $\chi^2$  is presented in Col. 6. The standard error  $\sigma$  is that of a fitting Gaussian function and is considered to contain all the effects, including random variations in the exact quasi-periodic oscillation, the large and changing width of the outburst structure, the poor coverage of some outbursts, the random variations in intensity, and in particular the intrinsic coherence of variability. To quantify the coherence of the variabilities, we calculate the quality factor  $Q = \nu/\text{HWHM}$  and give it in Col. 5, where HWHM is the half width at half maximum of a peak. The quality factor  $Q$  in Table 1 increases with the QPO frequency  $\nu$  and correlates with the repetitions of a QPO in the combined radio light curve, which is calculated with  $N = \nu\Delta T$ ,

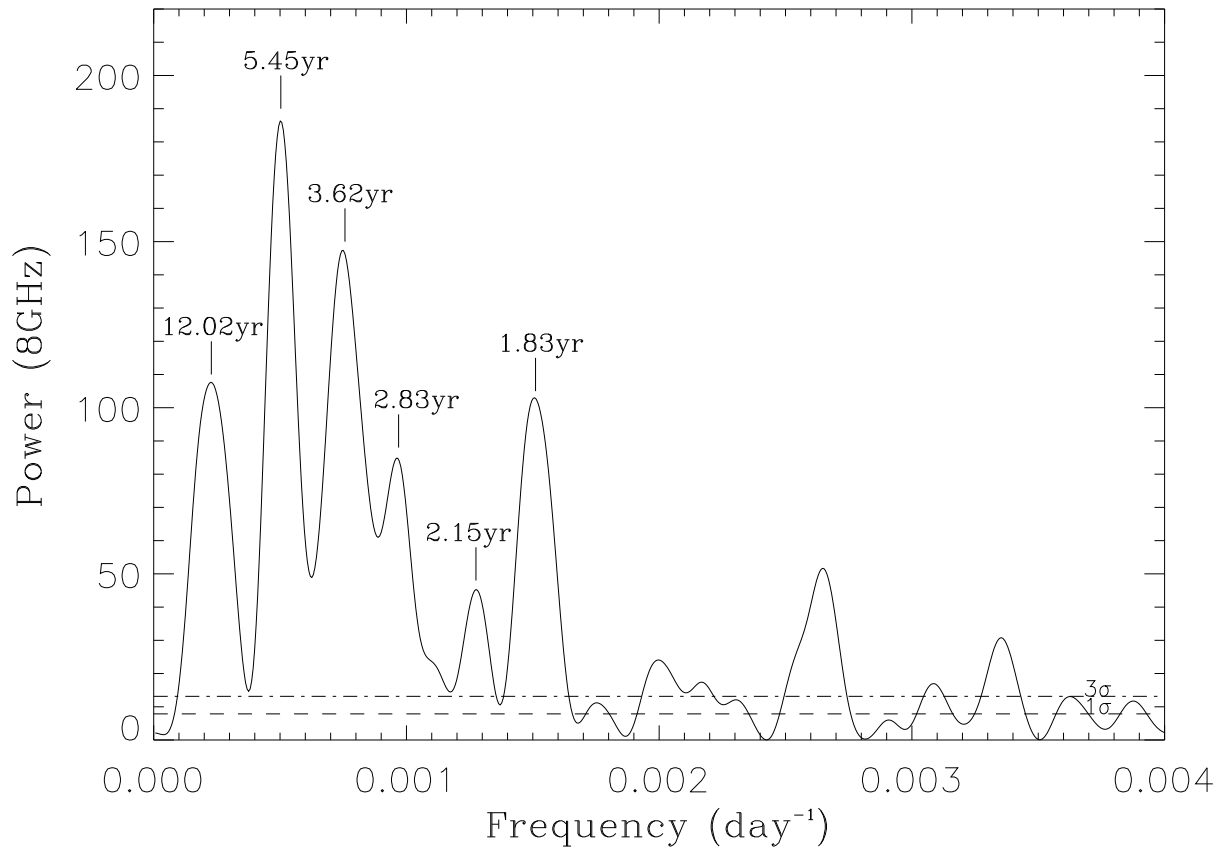


Fig. 2.— The power spectrum of the combined radio light curve at 8 GHz. Fitted centroid periods of QPOs are indicated. The dashed and the dash-dotted lines are the  $1\sigma$  and  $3\sigma$  significance levels, respectively.



where  $\Delta T \simeq 26.3$  yr is the total observation time of the combined data sample. A strong correlation of the quality factor  $Q$  and the repetition number  $N$  is showed in Fig. 4, implying that the coherence factor Q-value and the quality of QPOs are limited by the duration of the monitoring program. Therefore, to understand the intrinsic coherence of a QPO, we have to monitor the object for a much longer time.

In the Lomb periodogram of the combined 8 GHz light curve, we identify six QPOs of frequencies (periods)  $\nu_1 = 0.2279 \times 10^{-3} \text{ day}^{-1}$  ( $P_1 = 12.02$  yr),  $\nu_2 = 0.5029 \times 10^{-3} \text{ day}^{-1}$  ( $P_2 = 5.45$  yr),  $\nu_3 = 0.7568 \times 10^{-3} \text{ day}^{-1}$  ( $P_3 = 3.62$  yr),  $\nu_4 = 0.9691 \times 10^{-3} \text{ day}^{-1}$  ( $P_4 = 2.83$  yr),  $\nu_5 = 1.275 \times 10^{-3} \text{ day}^{-1}$  ( $P_5 = 2.15$  yr), and  $\nu_6 = 1.511 \times 10^{-3} \text{ day}^{-1}$  ( $P_6 = 1.81$  yr). The periods of the QPOs and the standard errors are given in Col. 4 of Table 1. To estimate the relative contribution of each QPO signal to the total flux variations, we compute the relative root mean square (*rms*) in percentage and give the results in Col. 3 of Table 1. The results show that the QPO of period  $P = 5.45$  yrs is the strongest with *rms*  $\sim 10$  per cent, though the other QPOs are also significant. We identify the frequency of the strongest QPO with the fundamental one with frequency  $\nu_s$ .

In order to confirm the detection of multiple QPOs, we now apply the least variance analysis introduced by Jurkevich (1971) and the z-transform discrete correlation function (ZDCF) technique (Alexander 1997) to the combined 8 GHz light curve. Jurkevich method has been successfully developed to search for periods in the optical light curves of some blazars (e.g. Kidger et al. 1992; Liu et al. 1995a, 1997). The method is based on the Expected Mean Square Deviation and specifically designed for the unevenly sampled datasets. It tests a run of trial periods. A light curve is first folded in a trial period and the variance  $V_m^2$  is computed first for each phase bin and then over a whole period. For a false trial,  $V_m^2$  is almost constant but for a true one it reaches a minimum. Instead of the normalized  $V_m^2$  itself, a parameter  $f = (1 - V_m^2)/V_m^2$  is usually introduced to described the significance of a period in a light curve (Kidger et al. 1992; Liu et al. 1995a). It is suggested that  $f > 0.25$  implies a strong period. A more general description and a robust test of the method was given by Liu et al. (1997). The analysis results with Jurkevich  $V_m^2$  method are given in Fig. 5. In the  $V_m^2$ -plot with very high signal-to-noise ratio, there are several very prominent minima with broad width at the trial periods  $P = 1.78$  yr, 3.46 yr, 5.34 yr, 7.90 yr, 11.60 yr and 15.10 yr. The last period may not be real, because it is very long and the data sample covers it less than two times. Among all the six QPOs detected with the Lomb power spectrum method, strong QPOs of periods  $P_1$ ,  $P_2$ ,  $P_3$ , and  $P_6$  with *rms* larger than 7 per cent are clearly detected by the Jurkevich  $V_m^2$  method, though the central frequencies of the periods shift toward to the lower end and cannot be determined accurately due to large noise. Weak QPOs  $\nu_4$  and  $\nu_5$  with *rms*  $\lesssim 6\%$  are insignificant in the normalized  $V_m^2$ -plot and are nearly drowned out by noise. In Fig. 5, a period  $P = 7.90$  yr is significant but not present in the

Lomb periodogram shown in Fig. 2. One possibility is that the QPO at  $P_1 = 12.02$  yr with low quality factor  $Q$  in the Lomb periodogram may consist of several QPOs (e.g. those periods  $P = 7.90, 11.6$  yr, and  $15.10$  yr in the normalized  $V_m^2$ -plot) and cannot be resolved due to the very low quality factor  $Q$ . However, it is more likely that the period  $P = 7.90$  yr in Fig. 5 does not represent a real QPO but just a spurious period at the position of two and four times of the two strong QPOs  $P_3 = 3.62$  yr and  $P_6 = 1.81$  yr, respectively. Or, the period  $P = 7.90$  yr is just the result of incorrect identification of noise.

We also analyze the combined radio light curve with the z-transform discrete correlation function (ZDCF) technique (Alexander 1997), which is designed properly to treat the unevenly sampled datasets. Discrete self-correlation function has been successfully used to search for periods in the light curves of AO 0235+164 (e.g. Raiteri et al. 2001) and ZDCF is basically the same as DCF. The self-ZDCF function of the combined radio light curve at 8 GHz is showed in Fig. 6. In self-ZDCF, a local maximum implies a period. In Fig. 6, all the maxima have very broad profile and the period is difficult to determine accurately. Because our purpose is to confirm the periodic analysis results obtained with the Lomb power spectrum method and the Jurkevich method, we do not try to compute periods from ZDCF accurately but estimate a period at peak. The identified five QPOs have periods  $P = 11.34$  yr,  $7.39$  yr,  $5.53$  yr,  $3.33$  yr,  $1.88$  yr. The periodic analysis results with the ZDCF and Jurkevich methods are consistent with each other within the estimate errors but not fully consistent with the results with the Lomb power spectrum method. Like the Jurkevich method, ZDCF does not detect the two weak periods  $P_4 = 2.83$  yrs and  $P_5 = 2.15$  yrs obtained with Lomb’s power spectrum method. It might be due to the broad profiles of the strong periods  $1.88$  yrs and  $3.33$  yrs at ZDCF and/or to the weakness of the two periods, so that the two weak QPOs are absent in the ZDCF.

The conclusions from three different periodic analysis methods are that the strong QPOs with periods  $P = 12.02, 5.45, 3.62,$  and  $1.81$  yrs are detected with unprecedentedly high signal-to-noise ratio in the combined 8 GHz radio light curves. Two weak QPOs with  $P = 2.83$  yr and  $2.15$  yr are detected by the Lomb power spectrum method but are not detected by the other two methods due to the weakness. They will be confirmed with the periodic investigation of radio light curves at multiple radio frequencies in Sec. 4.2.

## 4. Harmonic relationship and dependence of QPOs on radio frequencies

### 4.1. Harmonic relationship of QPOs

The ratio of centroid frequency and the fundamental frequency,  $f_\nu = \nu/\nu_s$ , of six QPOs is given in Col. 8 in Table 1. We do not compute the error for the ratio as the standard errors  $\sigma$  of the frequencies given in Col. 2 are limited by the time coverage of the data sample. The ratios  $f_\nu$  of six QPOs can be given with a simple relation  $f_\nu = I/2$  with  $I = 1, 2, 3, 4, 5,$  and  $6$ , or all six QPOs have harmonic relation  $\nu_1 : \nu_2 : \nu_3 : \nu_4 : \nu_5 : \nu_6 = 1 : 2 : 3 : 4 : 5 : 6$ . The identification is given in Col. 9 of Table 1. With the identification, we calculate the averaged fundamental frequency  $\bar{\nu}_s$  and the standard error  $\bar{\sigma}_s$  with  $\bar{\nu}_s = \bar{\sigma}_s \sum(\nu_j/\sigma_j)/N$  and  $1/\bar{\sigma}_s = \sum(j/\sigma_j)/2N$  with  $j = 2, \dots,$  and  $6$ , where  $N$  is the total number of QPOs used in the calculation. In the computation, we do not take into account the QPO with the lowest frequency  $\nu_1$  (the longest period  $P_1 = 12.02$  yr) due to the low quality factor  $Q = 1.76$ . The averaged frequency of the fundamental QPO is  $\bar{\nu}_s = (0.5014 \pm 0.0434) \times 10^{-3} \text{ day}^{-1}$  (period  $P_s = 5.46 \pm 0.47$  yr). With the least square method, we fit the combined 8 GHz radio light curve both with the fundamental QPO alone ( $\chi^2 = 0.7539$ ) and with the six detected QPOs ( $\chi^2 = 0.3235$ ), and give the results in Fig. 7. Fig. 7 shows that the fundamental QPO alone cannot satisfactorily reproduce the radio light curve while the fit with six QPOs can produce it very well until about the year 2000. The results imply that the contributions from the harmonic QPOs are significant, and the sub-peaks of the outbursts are not random but have the same physical origin as that of the major outbursts. The differences of the initial phases of six QPO harmonics relative to the fundamental are listed in the last column of Table 1. The results show that the QPOs  $\nu_1, \nu_2, \nu_3, \nu_5,$  and  $\nu_6$  almost have the same initial phases with  $\Delta\phi_0 \sim 0$  while  $\Delta\phi_0 \sim \pi$  for the 4th QPOs  $\nu_4$ . The initial phase difference  $\Delta\phi_0$  of the 1st and the 5th QPOs are deviated from zero because the large fit uncertainties due to the low quality factor  $Q$  for the 1st harmonics or to the weakness ( $rms = 4.70\%$ ) of the 5th harmonics, respectively. The relative initial phases of QPOs are consistent with the suggestion of a harmonic relationship among QPOs.

### 4.2. Frequency dependence of harmonic QPOs

In this section, we present QPO analyses with the radio light curves at 4.8 GHz, 14.5 GHz, 22 GHz, and 37 GHz and investigate the dependence of the harmonic QPOs on radio frequency. Since our purpose is to investigate the QPOs and the frequency dependence, we give only the analysis results with the Lomb power spectrum method. The radio data at 4.8 GHz and 14.5 GHz from UMRAO and at 22 GHz and 37 GHz from Metsähovi Observatory

are plotted in Fig. 7. The periodic analysis results are given in Fig. 8.

Fig. 8 shows that the Lomb periodograms of radio light curves at the four radio frequencies are very noisy and the signal-to-noises of the Lomb periodogram are significantly lower than that of the combined radio light curve at 8 GHz. Among six QPOs obtained at 8 GHz, the five strongest QPOs are detected in the radio light curves at all the radio frequencies, while the weakest QPO of period  $P_5 = 2.15$  yr and  $rms = 4.70$  per cent at 8 GHz is significantly detected only at 14.5 GHz, at which frequency the radio light curve is relatively well sampled. At 4.8 GHz, 22 GHz and 37 GHz, the weakest QPO is absent from the Lomb power spectra probably due to poor sampling and to the missing of the information on the minor events. Like at 8 GHz, the peak at a period with  $P \sim 7$  yr obtained both with the Jurkevich  $V_m^2$  and the ZDCF methods, is not present in the Lomb periodograms at all the radio frequencies in Fig. 8. Table 1 lists the fitted centroid frequency with Gaussian function, fitting goodness  $\chi^2$ , relative strength  $rms$ , quality factor  $Q$ , the ratio of the frequencies of harmonics and the fundamental QPOs, and the averaged fundamental period  $\bar{P}_s$ . Again, the QPOs clearly have a harmonic relationship and the identification of the harmonic integer is given in Table 1. Like what we did for the combined 8 GHz light curve, with the least square method we also fit the radio light curves at 4.8 GHz, 14.5 GHz, 22 GHz and 37 GHz both with the fundamental QPO  $\bar{\nu}_s$  alone and the six QPOs together, respectively. The fitted light curves are given in Fig. 7 and the differences of the initial phases of harmonic and the fundamental QPOs are listed in Col. 10 of Table 1. From the fitting results in Table 1, the differences of initial phases of the six QPOs at the four radio frequencies are consistent with the results obtained at 8 GHz and five QPOs  $\nu_1, \nu_2, \nu_3, \nu_5,$  and  $\nu_6$  have almost the same initial phases but about  $\pi$  difference from that of the 4th one. The results strongly support the identification of six QPOs and the harmonic relationship.

The dependence of QPO centroid frequency on the observational radio frequencies is given in Fig. 9. Fig. 9 shows that QPO frequencies are independent of the radio frequencies and the ratios of the frequencies of harmonic QPOs at the four radio wave-bands and the fundamental one with  $\nu_s = 0.5029 \times 10^{-3} \text{ day}^{-1}$  at 8 GHz are also independent of the radio frequencies, implying that the QPO centroid frequencies and the harmonic relationship are not determined by the different radio emission regions in relativistic jet. However, the independence does not mean that one could detect all the harmonic components of QPOs at all wave-bands. To answer this question, we investigate the dependence of relative amplitude  $rms$  on radio frequencies. Fig. 10 shows the results that the relative amplitude  $rms$  of all QPOs is a function of radio frequency and the third QPO has the strongest dependence. However, the conclusion is very sensitive to the periodic analysis results of radio light curves at 37 GHz, which is poorly sampled. Therefore, the decrease of QPO amplitudes may be due to the loss of information on high frequency QPOs in the poorly-sampled radio light curves.

To eliminate the effect of the incomplete coverage of outburst structures on the analysis results of QPO harmonic components, we calculate the ratio of  $rms$  of the harmonics and  $rms(\nu_s)$  of the fundamental QPO. The results are given in Fig. 10. In Fig. 10,  $rms/rms(\nu_s)$  for the 1st, 4th and 6th components of the harmonic QPOs is nearly independent of frequency while for the 3rd harmonics the ratio decreases with radio frequency. Again, the conclusion is sensitive to the periodic analysis results of the 37 GHz light curve. If the analysis results of QPOs at 37 GHz are not considered, the harmonics of QPOs are nearly independent of radio frequencies. The results suggest that if one detects the fundamental QPO of period  $P_s = 5.46$  yr in a well-sampled light curve at high frequency, e.g. in the optical wave-bands, one would simultaneously detect the other QPOs with periods  $P_1 \simeq 10.9$  yr,  $P_4 \simeq 2.8$  yr, and  $P_6 \simeq 1.8$  yr. But, the QPO of period  $P_3 = 3.6$  yr may not be observable in optical wave-band. Although the conclusion needs to be tested with much more observations at 37 GHz, our results suggest that the properties of QPOs would be independent of radio frequency and not be determined by the physical process in the radio emission regions of jet.

## 5. Central black hole mass and thick disk oscillations

Raiteri et al. (2001) reported the detection of a period  $P = 5.7 \pm 0.5$  yrs in the optical and radio light curves of AO 0235+164. Ostorero et al. (2004) interpreted it with a helical jet model, in which the quasi-periodic radio-optical light curve and the spectral energy distributions (SEDs) are caused by the orientation variation of a helical inhomogeneous, non-thermally emitting jet probably due to the orbital motion of the primary black hole in a binary system. In the helical jet model, the minor burst events are taken as non-periodic flux fluctuations due to the random plasma instabilities. However, our periodic analyses show that the major outbursts and the minor burst events are the products of combinations of six harmonic QPOs, which suggest a quasi-periodic radio emission from relativistic jets and a physical origin of harmonic QPOs independent of the radio emission regions in the jet. The multiplicity, the harmonic relationship, the zero differences of initial phases, and the independence of relative  $rms$  on radio frequency imply that the harmonic QPOs in the radio light curves of AO 0235+164 are most likely due to the quasi-periodic injection of plasma from accretion disk into the relativistic jet. Because of the jet-disk coupling (Fender & Belloni 2004), such a quasi-periodic plasma injection implies a quasi-periodic oscillation of accretion around SMBH.

Both thin and thick accretion disks can oscillate quasi-periodically, but only the oscillation of a thick disk can be global and trigger the quasi-periodic accretion with harmonic frequencies. Rezzolla et al. (2003a) and Zanotti et al. (2003) found that the accretion

rate of a tori or thick disk of finite radial extent is quasi-periodic due to the global p-mode oscillation, which could be excited by a global perturbation (Rezzolla et al. 2003b; Zanotti et al. 2003) or a local periodic strong agent (Rubio-Herra & Lee 2005a,b). Such a torus or thick disk of finite radial extent could be a optically thin and geometrically thick radiatively inefficient accretion flow (RIAF) or advection dominated accretion flow (ADAF) between a central supermassive black hole and an outer truncated geometrically thin disk. It is clear now that such a configuration should be present in a black hole accretion system if the dimensionless accretion rate  $\dot{m} \equiv \dot{M}/\dot{M}_{\text{Edd}}$  is lower than a critical value  $\dot{m}_{\text{cr}} \simeq 0.02$  (e.g. Meyer & Meyer-Hofmeister 1994; Narayan & Yi 1995; Narayan 2002; Esin et al. 1997; Meyer et al. 2000; Meyer-Hofmeister et al. 2005), where  $\dot{M}_{\text{Edd}} = L_{\text{Edd}}/0.1c^2$  is the Eddington accretion rate relative to the Eddington luminosity  $L_{\text{Edd}} \simeq 1.26 \times 10^{46} \text{ erg s}^{-1} (M/10^8 M_{\odot})$ . Because the p-mode oscillation frequency of thick accretion disk is determined by the disk radial extent defined with the dimensionless accretion rate, we now estimate the mass  $M_{\text{BH}}$  of central black hole and then the dimensionless accretion rate  $\dot{m}$  of AO 0235+164.

### 5.1. Black hole mass and accretion rate

As there is no valid estimation of the black hole mass of AO 0235+164 in literature, we estimate its black hole mass and the accretion rate in this section, before we start the investigations of the physical origin of QPOs. Because of the high redshift ( $z = 0.94$ ) and the very bright central nucleus, it is impossible to resolve the host galaxy of AO 0235+164 even with the Hubble Space Telescope and to infer the black hole mass with the tight relation of black hole mass and the properties of galaxy bulge (e.g. stellar velocity dispersion  $\sigma$ ). However, we can estimate the black hole mass with some recently suggested relations of the emission line properties and central black hole mass in AGNs.

The reverberation mapping studies reveal an empirical relation of broad emission line region (BLR) size and the optical continuum luminosity at rest-frame  $5100\text{\AA}$  (Kaspi et al. 2005)

$$\frac{R_{\text{BLR}}}{10 \text{ lt} - \text{days}} = (2.23 \pm 0.21) \left[ \frac{\lambda L_{\lambda}(5100\text{\AA})}{10^{44} \text{ ergs s}^{-1}} \right]^{0.69 \pm 0.05}. \quad (2)$$

Together with the FWHM of  $\text{H}_{\beta}$  emission line, which is a measurement of the characteristic velocity of broad emission line clouds, one can estimate the central black hole mass of an AGN with the relation (Peterson et al., 2004)

$$M_{\text{BH}} = 1.936 \times 10^5 M_{\odot} \left( \frac{R_{\text{BLR}}}{\text{lt} - \text{days}} \right) \left[ \frac{\text{FWHM}(\text{H}_{\beta})}{10^3 \text{ km s}^{-1}} \right]^2. \quad (3)$$

The environment of AO 0235+164 is rather complex due to the presence of several foreground intervening galaxies within a few arc-seconds. Great efforts have been done to study the emission line features of the object with spectroscopic observations. Using the 3m Shane telescope at Lick Observatory, Cohen et al. (1987) identified the emission lines of MgII, [NeV] and [OII] at the source red shift. With the 4m William Herschel Telescope, Nilsson et al. (1996) detected not only the [NeV] and [OII] lines but also prominent hydrogen emission lines  $H_\delta$  and  $H_\gamma$  at the same redshift. Nilsson et al. (1996) obtained the FWHM and flux (in the observer’s frame) of  $H_\delta(\lambda 4102)$  and  $H_\gamma(\lambda 4340)$  emission lines to be  $3600 \pm 400 \text{ km s}^{-1}$ ,  $39 \times 10^{-17} \text{ ergs}^{-1} \text{ cm}^{-2}$  and  $3400 \pm 400 \text{ km s}^{-1}$ ,  $97 \times 10^{-17} \text{ erg s}^{-1} \text{ cm}^{-2}$ , respectively. The equivalent widths of the  $H_\delta$  and  $H_\gamma$  lines are  $2.6 \text{ \AA}$  and  $7.2 \text{ \AA}$  (all the quantities are given in rest frame except noted). With the assumption of a power-law optical continuum ( $F_\nu \propto \nu^{-\alpha}$ ), we can estimate the flux at  $5100 \text{ \AA}$  from the flux in the bluer band. However, deriving an accurate value of spectral index  $\alpha$  is not a simple task for AO 0235+164 because of its strong variation (Smith et al. 1987). A visual inspection of Fig. 1 of Cohen et al. (1987) reveals that at  $4500 \text{ \AA}$  (observer’s frame) the continuum flux density is about  $0.5 \times 10^{-16} \text{ erg s}^{-1} \text{ cm}^{-2} \text{ \AA}^{-1}$ , while at  $7500 \text{ \AA}$  it is about  $1.1 \times 10^{-16} \text{ erg s}^{-1} \text{ cm}^{-2} \text{ \AA}^{-1}$ . From these flux values we can derive  $\alpha=3.54$ , which is in fair agreement with the values of  $\alpha \sim 3.6$  corresponding to a faint state of the source reported in Fig. 7 of Raiteri et al. (2001). However, when one takes into account the absorption by the intervening system at  $z=0.524$ , this value nearly halves. This can be inferred by the intrinsic (dereddened)  $\langle B - R \rangle = 1.72$  derived by Raiteri et al. (2005) which, when considering the amount of extra absorption tabulated in their Table 5, gives  $\langle \alpha \rangle = 1.75$ . We notice that this  $\alpha$  value means a relatively flat shape in the optical band of the flux density versus wavelength plot ( $F_\lambda \propto \lambda^{\alpha-2}$ ), which is also consistent with the dereddenned spectrum shown in Fig. 7 of Junkkarinen et al. (2004). Adopting  $\alpha=1.75$ , from the observed flux at  $7500 \text{ \AA}$  (rest-frame  $3866 \text{ \AA}$ ) in Fig. 1 of Cohen et al. (1987) we calculate the flux density at rest-frame  $5100 \text{ \AA}$  as  $7.5 \times 10^{-16} \text{ erg s}^{-1} \text{ cm}^{-2} \text{ \AA}^{-1}$ , while from the continuum flux at  $4102 \text{ \AA}$  estimated from the  $H_\delta$  line flux and equivalent width in Nilsson et al. (1996) we calculate the flux density at rest-frame  $5100 \text{ \AA}$  as  $5.3 \times 10^{-16} \text{ erg s}^{-1} \text{ cm}^{-2} \text{ \AA}^{-1}$ . From the average value of these two estimates, we obtain the monochromatic luminosity at  $5100 \text{ \AA}$  with  $\lambda L_\lambda(5100 \text{ \AA}) = 7.48 \times 10^{45} \text{ erg s}^{-1}$ . From Eq. (2), we estimate the BLR size as  $R_{\text{BLR}} = 438 \pm 103 \text{ lt - days}$ . Because of no detection of  $H_\beta$  for AO 0235+164 in literature, we try to estimate its FWHM from the observations of other Hydrogen Balmer lines. As the observed  $H_\gamma$  line is probably contaminated by [OIII]( $\lambda 4363$ ) line, we make the estimation with  $H_\delta$  line data. From the observations of 50 quasars in LBQS given by Forster et al. (2001), we derive an empirical relation between the FWHM values of  $H_\beta$  and  $H_\delta$  lines with the OLS bisector method (Isobe et al. 1990)

$$\text{FWHM}(H_\beta) = (415.6 \pm 348.8) + (1.07 \pm 0.15)\text{FWHM}(H_\delta). \quad (4)$$

From the observations of the FWHM of  $H_\delta$  line, we have  $\text{FWHM}(H_\beta) \simeq 4267 \pm 772 \text{ km s}^{-1}$  for AO 0235+164. From Eq. (3), we estimate the central black hole mass of AO 0235+164 to be  $M_{\text{BH}} \simeq (1.54 \pm 0.67) \times 10^9 M_\odot$ . However, AO 0235+164 is a blazar-type object and its optical continuum luminosity is generally dominated by the beamed synchrotron emission from a relativistic jet rather by the emission from accretion disk. The southern intervening galaxy with  $z=0.524$  may also partly contribute to the optical continuum luminosity (Nilsson et al. 1996). Therefore, the estimated black hole mass with the optical continuum luminosity is overestimated and can be taken only as an upper limit.

To avoid such an overestimation of black hole mass, Wu et al. (2004) argued that the emission line luminosity is probably a better tracer of the ionizing continuum luminosity of blazars and proposed a new empirical relation between the BLR size and the  $H_\beta$  emission line luminosity

$$\lg R_{\text{BLR}}(\text{lt} - \text{days}) = (1.381 \pm 0.080) + (0.684 \pm 0.106) \lg(L_{H_\beta}/10^{42} \text{ ergs s}^{-1}). \quad (5)$$

Because no detection of  $H_\beta$  emission line is reported for AO 0235+164 in literature, we estimate the luminosity from the observations of  $H_\delta$  and  $H_\gamma$  line fluxes. Zheng (1988) studied the variations of Balmer decrements of several quasars. From his table 2 and table 3, we get an averaged flux ratios 5 and 2.4 of  $H_\beta$  to  $H_\delta$  and  $H_\beta$  to  $H_\gamma$ , respectively. From the observations of emission lines by Nilsson et al. (1996), we obtain the rest-frame  $H_\beta$  luminosity for AO 0235+164 with  $L_{H_\beta} \simeq 1.68 \times 10^{43} \text{ ergs s}^{-1}$  from the observed flux of  $H\delta$  emission line. The estimated  $H_\beta$  luminosity from the observed  $H_\gamma$  flux is about 15 per cent higher, which might be due to the contamination of [OIII]( $\lambda 4363$ ) line. From Eq. (5) and the  $H_\beta$  luminosity estimated from  $H_\delta$  emission line flux, we calculate the BLR size as  $R_{\text{BLR}} = 166 \pm 64 \text{ lt} - \text{days}$ , which is much smaller than that estimated from the optical continuum luminosity. With the estimated BLR size and  $H_\beta$  FWHM value, from Eq. (3) we estimate the black hole mass of AO 0235+164 of  $M_{\text{BH}} = (5.85 \pm 3.09) \times 10^8 M_\odot$ , which is much smaller than that obtained with the optical continuum luminosity method.

McLure & Dunlop (2004) suggested to estimate the black hole mass of AGNs from the UV continuum luminosity and the FWHM of MgII(2788Å) emission line with an empirical relation (with cosmological parameter  $H_0 = 70 \text{ km s}^{-1} \text{ Mpc}^{-1}$ ,  $\Omega_{\text{m}} = 0.3$  and  $\Omega_{\Lambda} = 0.7$ ; the distance of AO 0235+164 is 6.1Gpc in this case)

$$M_{\text{BH}} = 3.2 M_\odot \left( \frac{\lambda L_{3000\text{\AA}}}{10^{44} \text{ ergs s}^{-1}} \right)^{0.62} \left[ \frac{\text{FWHM}(\text{MgII})}{\text{km s}^{-1}} \right]^2. \quad (6)$$

For AO 0235+164, the MgII emission line is observed to have the FWHM of  $3100 \text{ km s}^{-1}$  and the flux of  $1.24 \times 10^{-15} \text{ ergs cm}^{-2} \text{ s}^{-1}$  (Cohen et al. 1987). The equivalent width



and the continuum flux are  $15.7\text{\AA}$  and  $0.8 \times 10^{-16} \text{ ergs cm}^{-2} \text{ s}^{-1} \text{\AA}^{-1}$ , respectively. Using the observations of the MgII emission line and the continuum, we derive the rest-frame continuum luminosity at  $3000\text{\AA}$  of  $\lambda L_{3000\text{\AA}} = 7.37 \times 10^{45} \text{ erg s}^{-1}$  (using the same cosmological parameters as in McLure & Dunlop (2004)). From Eq. (6), we obtain a black hole mass  $M_{\text{BH}} = 4.42 \times 10^8 M_{\odot}$ , which is approximately the same as the estimation obtained with the luminosity of H $\beta$  emission line. However, the same as the optical continuum luminosity, the UV continuum luminosity of AO235+164 is also contributed by the jet emission and probably by the intervening galaxy. On the other hand, a recent study of Junkkarinen et al. (2004) indicated that the UV continuum of AO 0235+16 is heavily absorbed by the Galaxy and the intervening materials at  $z=0.524$ , which implies that the de-reddened UV continuum is much larger than the observed one (see their Fig. 7). Therefore, the UV continuum luminosity of AO 0235+164 suffers large uncertainties and the estimated black hole mass derived with it may be unreliable and will be considered only as a reference.

It has been found that there is a tight correlation between the black hole mass and the bulge velocity dispersion for nearby galaxies (Gebhardt et al. 2000; Merritt & Ferrarese 2001; Tremaine et al. 2002), which can be expressed as (Tremaine et al. 2002)

$$\text{Log}(M_{\text{BH}}/M_{\odot}) = 8.13 \pm 0.06 + (4.02 \pm 0.32) \text{ Log}(\sigma/200 \text{ km s}^{-1}). \quad (7)$$

AGNs seem to follow the same correlation as nearby galaxies (Ferrarese et al. 2001; Onken et al. 2004). On the other hand, there is also a tight correlation between the central velocity dispersion of galactic bulge and the FWHM of [OIII](5007 $\text{\AA}$ ) emission line in AGNs with  $\sigma \approx \text{FWHM}([\text{OIII}])/2.35$  (Nelson & Whittle 1995). This suggests that black hole mass could be roughly estimated from the observed FWHM values of narrow forbidden lines in AGNs. For AO 0235+164, both Cohen et al. (1987) and Nilsson et al. (1996) have detected narrow forbidden lines at redshift of  $z = 0.94$ . Cohen et al. (1987) estimated the FWHM values of [Ne V](3426 $\text{\AA}$ ) and [OII](3727 $\text{\AA}$ ) as  $600 \text{ km s}^{-1}$  and  $200 \text{ km s}^{-1}$ , respectively. Nilsson et al. (1996) obtained the FWHM values of [Ne V](3346 $\text{\AA}$ ), [Ne V](3426 $\text{\AA}$ ) and [OII] (3727 $\text{\AA}$ ) as  $700 \pm 100 \text{ km s}^{-1}$ ,  $400 \pm 100 \text{ km s}^{-1}$  and  $600 \pm 100 \text{ km s}^{-1}$ , respectively. From the emission line data of quasars in LBQS (Forster et al. 2001), we know that the average FWHM value of [OIII](5007 $\text{\AA}$ ) is comparable with those of [OII] (3727 $\text{\AA}$ ) and other narrow forbidden lines. Therefore we roughly take  $600 \text{ km s}^{-1}$  as the FWHM value of [OIII](5007 $\text{\AA}$ ). Using  $\sigma \approx \text{FWHM}([\text{OIII}])/2.35$ , we derive the value of a central velocity dispersion  $\sigma = 255 \text{ km s}^{-1}$ . From Eq. (7), we estimate the black hole mass of AO 0235+164 as  $M_{\text{BH}} \approx (3.58 \pm 2.65) \times 10^8 M_{\odot}$ , which is consistent with the value obtained with the H $\beta$ -luminosity.

We have adopted four different kinds of methods to derive the SMBH mass of AO 0235+16. Except the optical continuum luminosity method which apparently overestimates the SMBH mass, the other three methods give the SMBH mass in a range from  $3 \times 10^8 M_{\odot}$  to

$6 \times 10^8 M_\odot$ , with typical uncertainties of a factor of a few. In the following discussions, we take the averaged mass  $M_{\text{BH}} = (4.72 \pm 2.04) \times 10^8 M_\odot$  for the central black hole of AO 0235+164. However, we must keep in mind that the value is derived either with the indirect estimated  $\text{H}\beta$  and  $[\text{OIII}](5007\text{\AA})$  emission line properties or with the UV continuum luminosity which suffers from serious contaminations from the jet, southern intervening galaxy and extra-absorptions. In order to obtain more reliable black hole mass, further studies are absolutely needed to accurately determine the emission line and continuum properties of AO 0235+164.

Wang et al. (2004) calculated the broad line luminosity  $L_{\text{BLR}} \simeq 4.1 \times 10^{43} \text{ ergs s}^{-1}$  for AO 0235+164 (adjusted to fit the cosmological parameters used here). If we adopted a typical covering factor  $C \simeq 0.1$  for the broad-emission line region (Netzer 1990), the bolometric or the ionization luminosity is  $L_{\text{bol}} = L_{\text{ion}} \simeq L_{\text{BLR}}/C \simeq 4.1 \times 10^{44} \text{ ergs s}^{-1}$ . From the estimated bolometric luminosity and black hole mass, we obtain the dimensionless accretion rate  $\dot{m} \simeq 7 \times 10^{-3}(\eta/0.1)^{-1}$  of AO 0235+164, where  $\eta$  is the conversion efficiency of matter to energy.

## 5.2. Thick accretion disk p-mode oscillations and physical origin of multiple QPOs

The estimated dimensionless accretion rate of AO 0235+164 is about two times smaller than the critical accretion rate  $\dot{m}_{\text{cr}} \simeq 0.02$  in accretion disk evaporation model (Meyer et al. 2000; Liu et al. 2002) or much less than that of  $\dot{m}_{\text{cr}} \simeq 0.05$  in strong ADAF principle (Narayan & Yi 1995; Abramowicz et al. 1995), implying that the central region of the accretion disk in AO 0235+164 is in ADAF (or RIAF) and the outer region of the accretion disk is a truncated standard thin disk. There is no consensus in literature about how to determine the transition radius  $R_{\text{tr}}$  of inner thick ADAF and an outer thin standard disk. Three kinds of methods based on different physical processes have been proposed: disk evaporation (Meyer & Meyer-Hofmeister 1994; Liu et al. 1995b; Meyer et al. 2000; Liu et al. 2002; Róžańska & Czerny 2000), the absence of a strong ADAF solution (Narayan & Yi 1995; Abramowicz et al. 1995), and disk instability of inner radiation pressure dominated region with energy transfer outwards (Honma 1996; Kato & Nakamura 1998; Lu et al., 2004). The three methods generally give very different estimation of the transition radius. In the evaporation model, the transition radius at the critical accretion rate  $\dot{m}_{\text{cr}}$  is  $R_{\text{tr}} \simeq 355r_{\text{G}}$  (Meyer et al. 2000; Liu et al. 2002), while in the strong ADAF scenario, the transition radius at the critical accretion rate  $\dot{m}_{\text{cr}} \simeq 0.05$  is about  $R_{\text{tr}} \simeq 560r_{\text{G}}$  (Narayan & Yi 1995). The constraints from the existence of the broad line region in AGNs favored the relation of transition radius and accretion rate given by the strong ADAF principle (Czerny

et al. 2004).

In the strong ADAF scenario with advection fraction of energy  $f = 0.9$ , the relation of the transition radius and accretion rate for  $\dot{m} < \dot{m}_{\text{cr}}$  is  $R_{\text{tr}} \simeq 0.074 (\alpha/0.13)^4 \dot{m}^{-2} r_{\text{G}}$  (Narayan & Yi 1995), which gives a transition radius  $R_{\text{tr}} \simeq 1.5 \times 10^3 r_{\text{G}}$ . In the evaporation model (Meyer et al. 2000; Liu et al. 2002),

$$R_{\text{ev}} \simeq 18.3 \dot{m}^{-0.85} r_{\text{G}}, \quad (8)$$

which gives a consistent transitional radius  $R_{\text{tr}} = R_{\text{ev}} \simeq 1.2 \times 10^3 r_{\text{G}}$ .

Rezzolla et al. (2003b) and Zanotti et al. (2003) showed that if it is globally perturbed, a torus or a thick disk of finite radial extent oscillates globally. The global oscillations lead to quasi-periodic accretion with frequencies of harmonic relationship 1:2:3:4... (Zanotti et al. 2003)

$$f_m = m f_0, \quad (9)$$

where  $m = 1, 2, 3, \dots$ . The fundamental oscillation frequency  $f_0$  is given with  $f_0 = c_s/L$  where  $c_s$  is sound speed and  $L = p/(dp/dr)$  is the radial length scale of pressure  $p$ . Note that  $f_m$  in Zanotti et al. (2003) relates to the thick disk eigen-frequencies  $f_n = [(2+n)/2]f_0$  for  $n = 0, 2, 4, \dots$  and  $m = (2+n)/2$  (Rezzolla et al. 2003b). Therefore, the trapped acoustic wave should have zero initial phase difference. The quasi-periodic p-mode oscillations of a small-size torus orbiting around a black hole have been suggested to explain the high-frequency QPOs (HFQPOs) in black hole X-ray binary systems (Rezzolla et al. 2003a), which is observed to be in ratios of small integers (e.g. Abramowicz & Kluzniak 2001). If the inner thick accretion flow of finite radial size in AO 0235+164 is perturbed by global perturbation or by strong local periodic agent, the accretion rate would vary quasi-periodically, triggering quasi-periodical plasma injection into relativistic jet due to jet-disk coupling and leading to the quasi-periodical variation of jet emission. As it describes an ADAF quite well except at two boundaries, the self-similar solution of ADAF is used in estimation of the fundamental oscillation frequency  $f_0$ . From the self-similar solution for the ratio of specific heats  $\gamma = 5/3$  (Narayan & Yi 1994; Narayan et al. 2000), the pressure  $p \propto \rho c_s^2 \propto R^{-5/2}$  and sound speed  $c_s = \frac{\sqrt{10}}{3\alpha} \left[ \left(1 + \frac{18\alpha^2}{25}\right)^{1/2} - 1 \right]^{1/2} v_{\text{K}} \simeq (2/5)^{1/2} v_{\text{K}}$  for  $\alpha^2 \ll 1$ , where  $v_{\text{K}}$  is the Keplerian velocity at radius  $R$ . Then the fundamental frequency is

$$\begin{aligned} f_0 &= c_s/L \simeq (5/2)^{1/2} \Omega_{\text{K}} \\ &\simeq 1.13 \text{ yr}^{-1} \left( \frac{R}{10^3 r_{\text{G}}} \right)^{-3/2} \left( \frac{M_{\text{BH}}}{10^8 M_{\odot}} \right)^{-1}, \end{aligned} \quad (10)$$

where  $\Omega_{\text{K}}$  is the Keplerian angular frequency and  $r_{\text{G}} = 2GM/c^2 = 2.95 \times 10^{13} \text{ cm } (M/10^8 M_{\odot})$  is the Schwarzschild radius. The fundamental oscillation frequency of the thick ADAF of

AO 0235+164 is  $f_0 \simeq 0.182 \text{ yr}^{-1} (R_{\text{tr}}/1.2 \times 10^3 r_{\text{G}})^{-3/2} (M_{\text{BH}}/4.72 \times 10^8 M_{\odot})^{-1}$  and the fundamental period is  $P_0 = 5.48 \text{ yr} (R_{\text{tr}}/1.2 \times 10^3 r_{\text{G}})^{3/2} (M_{\text{BH}}/4.72 \times 10^8 M_{\odot})$ . The oscillation model for torus or thick disk predicts a series of overtones in a sequence 1:2:3:..., independent of the disk radial extent and of the variation of sound speed with radius. The fundamental frequency and all the overtones are predicted to have nearly zero initial phase difference.

With the redshift  $z = 0.94$  of AO 0235+164, we have the expected lowest frequency  $f_{\text{obs}} = f_0/(1+z) \simeq 2.57 \times 10^{-4} \text{ days}^{-1} (R_{\text{tr}}/1.2 \times 10^3 r_{\text{G}})^{-3/2} (M_{\text{BH}}/4.72 \times 10^8 M_{\odot})^{-1}$  and period  $P_{\text{obs}} \simeq 10.7 \text{ yr} (R_{\text{tr}}/1.2 \times 10^3 r_{\text{G}})^{3/2} (M_{\text{BH}}/4.72 \times 10^8 M_{\odot})$ , respectively, which are consistent with the detected frequency  $\nu_1 \simeq (2.28 \pm 1.10) \times 10^{-4} \text{ days}^{-1}$  and period  $P_1 \simeq (12.0 \pm 5.8) \text{ yrs}$  (or  $2P_2 = 10.9 \text{ yr}$  at higher accuracy) at 8 GHz and other radio frequencies. As the observed lowest frequency, the harmonics and the difference of initial phases are consistent with the predictions of a thick ADAF oscillation model, we suggest that the multiple harmonic QPOs in the radio light curves of AO 0235+164 are due to the perturbed p-mode oscillations of an ADAF with a finite radial extent  $R_{\text{tr}} \simeq 1.2 \times 10^3 r_{\text{G}}$  between a central supermassive black hole and an outer cool thin disk.

There are two difficulties needed to be addressed with the model. The first one is the relative strength of QPOs in the power spectrum. In the theoretical power spectrum of oscillation accretion, the fundamental QPO is the strongest and the strength of harmonics decreases with the oscillation frequency (Rezzolla et al. 2003b; Zanotti et al. 2003). The Lomb power spectrum periodic analyses show that the *rms* of QPOs indeed decreases with frequency except the 6th harmonics with frequency  $\nu_6 = (1.511 \pm 0.099) \times 10^{-3} \text{ day}^{-1}$  or period  $P_6 = 1.81 \pm 0.12 \text{ yr}$ , which is exceptionally prominent and inconsistent with the prediction of the disk oscillation model. The other is on the nature of perturbation source. There is no obvious global or local perturbation source in a SMBH-thick disk system in AO 0235+164. We will discuss the two difficulties in Sec. 6.

## 6. Perturbation sources and supermassive black hole binary

Although in Sec. 5.2 we suggest that the observed multiple harmonic QPOs in AO 0235+164 would be due to the p-mode oscillations of a thick accretion disk (ADAF or RIAF), the nature of strong excitation mechanisms, either local (Rubio-Herra & Lee 2005a,b) or global (Zanotti et al. 2003; Rezzolla et al. 2003a), is still an open question, in particularly for a system of a thick disk with large radial extent around a SMBH. Here we suggest that a SMBHB embedding in the thick accretion disk would serve as such a local, strong and periodic perturbation source as required by the p-mode oscillations of a thick accretion disk investigated by Rubio-Herra & Lee (2005b). A SMBHB may form in galaxy minor merger

and is introduced in a helical jet model for AO 0235+164 (Ostorero et al. 2004) and later in explaining the rapid changes in the VLBI (Very Long Baseline Interferometry) jet position angles of the radio source (Frey et al. 2006). A SMBHB embedding in an ADAF or RIAF cannot open a gap in an accretion disk, because to open a gap the disk opening angle  $H/R$  should be  $H/R \lesssim 0.3$  and the mass ratio  $q$  of the secondary and the primary black holes should be  $q \leq 1$  and  $q > q_{\min} = (81\pi/8)\alpha(H/R)^2 \gtrsim 3$  for an ADAF with  $H/R \sim 1$  and  $0.1 < \alpha < 0.3$  (Lin & Papaloizou 1986). The interaction with an RIAF is hydro-dynamically unimportant to the evolution of a SMBHB (Liu 2004), but the gravitational attraction of the secondary to the plasma in the thick disk changes periodically and triggers a series of density waves which propagate inwards and outwards in the thick disk with a limited radial extent. When they arrive at the inner or the outer boundaries, the acoustic waves are reflected backwards with a very large fraction of the incoming energy, if the acoustic frequency is about the fundamental frequency or harmonics of the cavity. Other acoustic waves are almost completely be absorbed by the boundaries. This kind of p-mode oscillations in a tours or thick accretion disk were first discussed for global perturbation by Rezzolla et al. (2003b) and later for local strong periodic agent by Rubio-Herra & Lee (2005a). A SMBHB thus perfectly serves as a local strong perturbation agent to a SMBH-thick disk system.

For a SMBHB with separation  $a \lesssim R_{\text{tr}}$ , the orbital period  $P_b$  should be

$$\begin{aligned} P_b &= 2\pi \left[ \frac{a^3}{GM_{\text{BH}}(1+q)} \right]^{1/2} \\ &\lesssim 8.8 \text{ yr} \left( \frac{R_{\text{tr}}}{10^3 r_G} \right)^{3/2} \left( \frac{M_{\text{BH}}}{10^8 M_\odot} \right) (1+q)^{-1/2}. \end{aligned} \quad (11)$$

In the observer’s frame, the period is observed to be  $P_{\text{obs}} = (1+z)P_b \lesssim 80 \text{ yr}$ , which may or may not be within the detection window of the three databases which we used. Rubio-Herra & Lee (2005b) showed that in addition to the strong QPO with very high quality factor  $Q$  at the perturbation period  $P_b$ , the oscillations of a perturbed thick disk should be detected significantly at  $P_b/2$  and possibly also at  $2P_b$ . In the helical-jet model (Ostorero et al. 2004), the SMBHB orbital period is identified with  $P_{\text{obs}} = P_2 \sim 5 - 6 \text{ yrs}$ . If the helical jet model is correct, the SMBHB has a separation  $a \simeq 166 r_G$ , which is much smaller than the transitional radius  $R_{\text{tr}}$  and implies an embedding SMBHB in ADAF (or RIAF). In this scenario, SMBHB should excite thick disk oscillations not only at period  $P_2$  but also at periods  $P_4$  and probably  $P_1$ . One difficulty with the explanation is that one has to explain the exceptional prominence of the 6th QPO with very high quality factor  $Q$ , which should be the weakest among six QPOs and may not be detectable in the disk oscillation model. Therefore, a more reasonable suggestion would be that the 6th QPO of period  $P_6 = 1.81 \text{ yr}$  corresponds to the SMBHB orbital motion. In this scenario, a QPO at period  $P_6/2 = 0.91 \text{ yrs}$

should also be significant, which might have already been detected with  $P = 1.03 \pm 0.03$  yrs at the Lomb power spectrum at 8 GHz in Fig. 2. However, a QPO with a period about one year may not be identified correctly due to the one-year astronomical cycle.

For a SMBHB with an orbital period  $P_{\text{obs}} = 1.81$  yr or 5.46 yr, the binary separation is

$$\begin{aligned} a &= r_G \left[ \frac{P_{\text{obs}}}{(1+z) 2\sqrt{2\pi} r_G} \frac{c}{r_G} \right]^{2/3} (1+q)^{1/3} \\ &\simeq 166 r_G (1+q)^{1/3} \quad \text{if } P_{\text{obs}} = 5.46 \text{ yr, or} \\ &\simeq 79 r_G (1+q)^{1/3} \quad \text{if } P_{\text{obs}} = 1.81 \text{ yr.} \end{aligned} \quad (12)$$

Because the interaction with an ADAF or RIAF is negligible and the evolution of SMBHB is dominated by the gravitational wave radiation (Liu 2004), the lifetime of SMBHB with a circular orbit in AO 0235+164 due to the gravitational wave radiation is (Peters & Mathews 1963)

$$\begin{aligned} t_{\text{gw}} &= \frac{a}{|\dot{a}|} = \frac{5}{8} \left( \frac{a}{r_G} \right)^4 q^{-1} (1+q)^{-1} \frac{r_G}{c} \\ &\simeq 7.0 \times 10^6 \text{ yr} \left( \frac{q}{0.01} \right)^{-1} (1+q)^{1/3} \quad \text{if } P_{\text{obs}} = 5.46 \text{ yr, or} \\ &\simeq 3.6 \times 10^5 \text{ yr} \left( \frac{q}{0.01} \right)^{-1} (1+q)^{1/3} \quad \text{if } P_{\text{obs}} = 1.81 \text{ yr.} \end{aligned} \quad (13)$$

Both identifications of the SMBHB orbital motion suggest a short-lived binary. However, it is also possible that the separation of SMBHB is  $a \sim 10^3 r_G$  and the orbital period  $P_b \sim 70$  yr is out of the observational window. A SMBHB with such a large separation is long-lived with  $t_{\text{gw}} \simeq 9.2 \times 10^9 \text{ yr} \left( \frac{q}{0.01} \right)^{-1} (1+q)^{1/3}$ . The observations of the changes of VLBI jet positional angle may help to resolve the puzzles.

## 7. Discussions and conclusions

We have investigated the radio variabilities of AO 0235+164 and analyzed the periods of radio light curves at 4.8, 8, 14.5, 22, and 37 GHz, basing on the databases of UMRAO, NRAO and Metsähovi Observatory. We first study the consistence of the UMRAO's and NRAO's data at 8 GHz for AO 0235+164 and then construct a combined radio light curve with the observational data from the two databases. The periodic analyses with three kinds of classical periodic analysis methods show with unprecedentedly high signal-to-noise ratio that the variations of the combined radio light curves are composed of six periodic variations plus random fluctuations. In the power spectrum, the peaks are Gaussian and identified with QPOs of periods  $P_1 = 12.02$  yr,  $P_2 = 5.45$  yr,  $P_3 = 3.62$  yr,  $P_4 = 2.83$  yr,  $P_5 = 2.15$  yr, and

$P_6 = 1.81$  yr. The coherent quality factor  $Q$  of the six QPOs are limited by the monitoring program time. We discover a harmonic relationship for the six QPOs, based on the ratio of QPO frequencies in a sequence of small integers 1:2:3:4:5:6 and on the zero or  $\pi$  difference of initial phases of QPOs. The harmonic relationship suggests that the six QPOs should have the same physical origin. Among the six harmonic QPOs, the second one with period  $P_2 \simeq 5.46 \pm 0.47$  yrs is the strongest and is identified with the fundamental period. The five strong harmonics reported in some literature are confirmed here with an unprecedentedly high signal-to-noise and accuracy, while the weakest QPO of period  $P_5 = 2.15$  yrs is reported first time in this paper.

We investigate the dependence of harmonic relationship, coherent quality factor, the relative *rms*, the differences of the initial phase of QPOs on radio frequency. The results show that all the QPO properties are independent of radio frequencies. The six harmonic QPOs give a good fit to the outburst structures of the radio light curves at 4.8, 8, 14.5, 22 and 37 GHz, and predict major outbursts and outburst structures significantly different from that given with a single period of  $P \simeq 5.46$  yr (Raiteri et al. 2001). Both the single-period and the multiple harmonic QPO (for the low frequencies) scenarios predict a major outburst in the early half of 2004, while the combinations of six harmonic QPOs suggest only minor fluctuations during that period but a major burst in the late half of 2004 or the early half 2005 at 37 GHz, as it is shown in Fig. 7. In our periodic analyses of radio light curves at 22 GHz and 37 GHz, we have used the data after 2001 and the harmonic QPO scenario predict a major outburst in the early 2005. At lower frequencies we cannot get the observational data in recent years and make the analyses basing on the data before 2001. Therefore, the predictions are slightly different for different wave-bands and the predicted major bursts may be in the early 2005. However, the observations of a WEBT (the Whole Earth Blazar Telescope) campaign started from 2003 show that AO 0235+164 is quiet in recent years and the predicted major outbursts in the spring of 2004 did not come (Raiteri et al. 2005). Is the predicted major outburst just delayed significantly or is the activity of the object interrupted due to some reasons? When will the object re-activate with a different active cycle? To answer the questions, more observations for another several years are needed.

Either a significant delay of outbursts or the interruption of activity for some time would exclude the single period scenario and the simple version of a helical jet model but may be consistent with the SMBHB-thick disk oscillation model. In a SMBHB-thick disk oscillation scenario, the multiple QPOs in the radio light curves of AO 0235+164 are due to quasi-periodic injection of plasma from an oscillation thick disk of a finite radial extent into relativistic jet. A torus or a thick accretion disk of finite radial extent oscillates and accretes matter quasi-periodically with small integer ratio of frequencies with 1:2:3:.., if it is perturbed by a global perturbation or a local strong periodic agent (Zanotti et al. 2003;

Rezzolla et al. 2003a; Rubio-Herra & Lee 2005b). The fundamental oscillation frequency of a thick disk is determined by the radial extent and sound speed. We estimated the central black hole mass  $M_{\text{BH}} = (4.72 \pm 2.04) \times 10^8 M_{\odot}$  and the dimensionless accretion rate  $\dot{m} \simeq 0.007$  of AO 0235+164, based on the observations of emission line properties. The estimated dimensionless accretion rate with the current knowledge of accretion around black hole suggests that the inner region of accretion disk in AO 0235+164 is a geometrically thick disk (i.e. ADAF or RIAF) with radial extent about  $1.2 \times 10^3 r_{\text{G}}$  and the outer region is a truncated cool thin disk. With the self-similar solution of ADAF, we analytically estimate the fundamental oscillation frequency  $f_{\text{obs}} \simeq 0.0938 \text{ yr}^{-1}$  or period  $P_{\text{obs}} = 10.7 \text{ yr}$  in the observer's frame, which together with the predicted overtones are consistent with the observed multiple QPOs with lowest frequency  $P_1 \simeq 12.02 \pm 5.79 \text{ yr}$  (or  $2P_2 = 10.9 \text{ yrs}$  at higher accuracy) and harmonics. As there is no natural global or strong local perturbation source in standard SMBHB-accretion disk system to excite the global oscillations of a thick disk of a large radial extent  $R_{\text{d}} \sim 10^3 r_{\text{G}}$ , we suggest a SMBHB rotating within the thick disk to excite the p-mode oscillations of RIAF in AO 0235+164. The rotation of the secondary triggers acoustic waves in an ADAF (or RIAF), which propagate inwards and outwards in the thick disk and are reflected backwards by the inner and outer boundaries. The p-mode oscillations with frequencies of about the fundamental oscillation frequency and the overtones are trapped by the cavity. The orbital motion of a SMBHB could lead to the formation of a helical morphology of relativistic jet and to the rapid changes of VLBI jet position angles. Therefore, in the SMBHB-disk oscillation model, the relativistic jet can be also helical. The orbital motion may correspond to the 6th QPO with  $P_6 = 1.81 \text{ yrs}$ , the 2nd QPO with  $P_2 = 5.46 \text{ yrs}$ , or have not been observed. Long term VLBI monitoring of rapid changes of jet positional angles would help to answer the question. One of the differences with the simple helical jet model is that in the SMBH-thick disk oscillation scenario the minor burst events in the radio light curves is no longer random but together with the major outbursts are the combinations of harmonic six QPOs which are the p-mode oscillations of the RIAF and the binary orbital motion. This is a first time report of multiple harmonic QPOs and the possible detection of perturbed disk p-mode oscillations in AGNs.

The second difference of predictions of the helical jet model and the SMBHB-thick disk oscillation scenario is that periodic outbursts in the former model are persistent and regular while in the later scenario are temporary with moderate coherence quality factor  $Q$  and depend on the dimensionless accretion rate. In the SMBHB-thick oscillation scenario, resonant harmonic QPOs would disappear from the radio light curves or the periodic activities of the radio source are interrupted, when the accretion rate increases only about two times and becomes larger than the critical accretion rate  $\dot{m}_{\text{cr}}$  and the inner region of accretion disk becomes a geometrically thin cool disk. Therefore, the quiescence and the absence of



outbursts from the radio light curves of AO 0235+164 may be because of the transition of accretion mode from a RIAF to a standard thin cool accretion disk due to the moderate increase of accretion rate. The X-ray spectral observations with the Chandra satellite in August 2000 and with the XMM-Newton satellite in August 2004 show tentative detections of the red-shifted Fe  $K\alpha$  fluorescent emission line in AO 0235+164 (Raiteri et al. 2006), which suggests that the accretion disk at the immediate vicinity of the SMBH is very likely a standard thin accretion disk (Fabian et al. 2000). Therefore, the absence of outbursts from the radio light curves and the interruption of the harmonic QPOs can be understood in the SMBHB-thick disk oscillation scenario as the transition of accretion mode due the increase of accretion rate. In a jet-disk coupling scenario, an object becomes radio quiet when the accretion disk becomes a standard thin disk (Fender & Belloni 2004).

We notice that in the helical jet model, the separation of SMBHB is much smaller than the transitional radius  $R_{\text{tr}}$  of inner thick RIAF and outer thin disk. Therefore, the SMBHB in the helical jet model for AO 0235+164 should also excite the p-mode oscillations of an RIAF, leading to quasi-periodic accretion and quasi-periodic injection of plasma into the relativistic jet. Therefore, multiple QPOs with harmonic relationship are also expected by the helical jet model for AO 0235+164, if we consider the RIAF p-mode oscillations.

The embedding secondary black hole spherically accretes matter from the RIAF and radiates energy in X-ray. The accretion radius of the secondary black hole is  $r_{\text{acc}} \approx \frac{Gm}{c_s^2 + (\Delta v)^2}$ , where  $\Delta v$  is the differential velocity of the secondary black hole and the plasma in the thick disk. For a minor merger with  $q \ll 1$ , we obtain  $r_{\text{acc}} \ll R$  and  $(\Delta v)^2 \ll c_s^2$ . From the self-similar solution  $c_s^2 = (2/5)V_K^2$  for  $\gamma = 5/3$  (Narayan & Yi 1994; Narayan et al. 2000), we have  $r_{\text{acc}} \approx (5/2)q(1+q)R$ . The accretion rate of the secondary black hole is

$$\dot{M}_s \sim 4\pi r_{\text{acc}}^2 c_s \rho, \quad (14)$$

where the mass density  $\rho$  is given with the self-similar solution and  $\rho = \frac{5\sqrt{5}}{12\sqrt{2}\pi} \dot{M}_{\text{Edd}} \dot{m} \alpha^{-1} R^{-2} V_K^{-1}$ . From Eq. (14), we have  $\dot{M}_s \sim \frac{25\sqrt{5}}{6\sqrt{2}} q^2 (1+q)^2 \dot{M}_{\text{Edd}} \dot{m} \alpha^{-1}$ . Defining the Eddington accretion rate for the secondary black hole  $\dot{M}_{\text{Edd}}^s = L_{\text{Edd}}^s / 0.1c^2$  with  $L_{\text{Edd}}^s = 1.26 \times 10^{38} (m/M_\odot) \text{ ergs s}^{-1}$ , we have the dimensionless accretion rate of the secondary black hole,  $\dot{m}_s \equiv \dot{M}_s / \dot{M}_{\text{Edd}}^s \sim 6.6(1+q)^2 (q/\alpha) \dot{m}$ . For the typical parameters  $q = 0.01$  and  $\alpha = 0.13$ , the relative accretion rate of the secondary is  $\dot{m}_s \sim 0.51\dot{m} \sim 5.1 \times 10^{-3}$ , while  $\dot{m}_s \sim 5.1 \times 10^{-2}$  for  $q = 0.1$ . The X-ray emission from the accretion of the secondary black hole is small and may not be observable in AO 0235+164, because of the strong X-ray radiations both from the relativistic jet and from accretion disk around the primary. A different  $\gamma$  value does not change the conclusion.

Our work implies that if a thick accretion disk with finite radial extent is perturbed

globally or locally by, e.g. SMBHB, the p-mode oscillations can be observed as multiple harmonic QPOs, when the relativistic jet is along the line of sight. Periods have been reported and SMBHBs have been suggested in literature for many AGNs. So, multiple QPOs with a harmonic relationship of frequencies are expected by the SMBHB-disk oscillation model in moderately low luminosity AGNs with SMBHB at center, which may have accretion configuration like the one in the BL Lac object AO 0235+164. We will report our periodic analysis results on a large sample of AGNs in a coming paper (Zhao, Liu, & Wu 2006).

We are grateful to L. Rezzolla, J. Miller, H. Su, R. Wang, X. Chen, Y.B. Liu, and B.F. Liu for many insightful discussions and help. Many thanks are due to the referee for his/her constructive comments, which help us to improve the presentations significantly. We thank Kari Nilsson for helpful explanations on the spectroscopic data of AO 0235+164. This work is supported by the National Science Foundation of China (No. 10203001, No. 10573001, No. 10473001, No. 10525313) and partly by the National Key Project on Fundamental Researches (TG 1999075403). This research has made use of:

–the data from the University of Michigan Radio Astronomy Observatory, which is supported by the National Science Foundation and by funds from the University of Michigan; and

–the data from the Green Bank Interferometer (GBI), National Radio Astronomy Observatory (NRAO). The Green Bank Interferometer is a facility of the National Science Foundation operated by the NRAO in support of NASA High Energy Astrophysics programs.

## REFERENCES

- Abraham Z., Romero G.E., 1999, *A&A*, 344, 61
- Abramowicz M.A., Chen X., Kato S., Lasota J.-P., Regev O., 1995, *ApJ*, 438, L37
- Abramowicz M.A., Kluźniak W., 2001, *A&A*, 374, L19
- Abramowicz M.A., Kluźniak W., 2004, *AIP Conf. Proc. Vol.714*, AIP, New York, p.21
- Alexander T. 1997, in *Astronomical Time Series*, ed. D. Maoz, A. Sternberg, & E. M. Leibowitz (Dordrecht: Kluwer), 163
- Aller H. D., Aller M. F., Latimer G. E., Hodge P. E. 1985, *ApJS*, 59, 513

- Aller M.F., Aller H.D., Hughes P.A., Latimer G.E., 1999, *ApJ*, 512, 601
- Antonucci R. 1993, *ARA&A*, 31, 473
- Begelman M.C., Blandford R.D., Rees M.J., 1980, *Nature*, 287, 307
- Cohen R.D., Harding E.S., Junkkarinen V.T., & Burbidge E.M. 1987, *ApJ*, 318, 577
- Czerny B., Róžańska A., Kuraszkiewicz J., 2004, *A&A*, 428, 39
- Esin A.A., McClintock J.E., Narayan R., 1997, *ApJ*, 489, 865
- Fabian A.C., Iwasawa K., Reynolds C.S., Young A.J., 2000, *PASP*, 112, 1145
- Falcke H., Mannheim K., Biermann P.L., 1993, *A&A*, 278, L1
- Fender R., & Belloni T., 2004, *ARA&A*, 42, 317
- Fender R.P., Belloni T.M., Gallo E., 2004, *MNRAS*, 355, 1105
- Ferrarese L., Pogge R.W., Peterson B.M., Merritt D., Wandel A., Joseph C.L. 2001, *ApJ*, 555, L79
- Fiedler R. L., Waltman E. B., Spencer J. H., Johnston K. J., Angerhofer P. E., et al. 1987, *ApJS*, 65, 319
- Forster K., Green P.J., Aldcroft T.L., Vestergaard M., Foltz C.B., & Hewett P.C. 2001, *ApJS*, 134, 35
- Frey S., Gurvits L.I., Gabuzda D.C., Salter C.J., Altschuler D.R., et al., 2006, *PASJ*, 58, 217
- Gallo E., Fender R.P., Pooley G.G., 2003, *MNRAS*, 344, 60
- Gebhardt K., Bender R., Bower G., Dressler A., Faber S. M., et al. 2000, *ApJ*, 539, L13
- Hasinger G., Langmeier A., Sztajno M., Truemper J., Lewin W.H.G., 1986, *Nature*, 319, 469
- Honma F., *PASJ*, 48, 77
- Isobe T., Feigelson E.D., Akritas M.G., & Babu G.J. 1990, *ApJ*, 364, 104
- Junkkarinen V.T., Cohen R.D., Beaver E.A., Burbidge E.M., Lyons R.W., Madejski G., 2004, *ApJ*, 614, 658
- Jurkevich I. 1971, *Ap&SS*, 13, 154

- Kaspi S., Maoz D., Netzer H., Peterson B.M., Vestergaard M., Jannuzi B.T., 2005, *ApJ*, 629, 61
- Kaspi S., Smith P.S., Netzer H., Maoz D., Jannuzi B.T., & Giveon, U. 2000, *ApJ*, 533, 631
- Kato S., 2005, *PASJ*, 57, L17
- Kato S., Nakamura K.E. 1998, *PASJ*, 50, 559
- Katz J.I., 1997, *ApJ*, 478, 527
- Kauffmann G., Haehnelt M., 2000, *MNRAS*, 311, 576
- Kidger M. R., Takalo L., Sillanpää A., 1992, *A&A*, 264, 32
- Komossa S., 2003, in Centrella J., ed., *AIP Conf. Proc.* 686, *The Astrophysics of Gravitational Wave Sources*. AIP, New York, p. 161
- Lainela M., Takalo L.O., Sillanpää A., et al., 1999, *ApJ*, 521, 561
- Lazio T.J.W., Waltman E.B., Ghigo F.D., Fiedler R.L., Foster R.S., Johnston K.J., 2001, *ApJS*, 136, 265
- Lehto H.J., Valtonen M.J., 1996, *ApJ*, 460, 207
- Lin D.N.C., Papaloizou J., 1986, *ApJ*, 309, 846
- Liu B.F., Mineshige S., Meyer F., Meyer-Hofmeister E., Kawaguchi T., 2002, *ApJ*, 575, 117
- Liu F.K., 2004, *MNRAS*, 347, 1357
- Liu F.K., Liu B.F., Xie G.Z., 1997, *A&AS*, 123, 569
- Liu F.K., Meyer F., Meyer-Hofmeister E., 1995b, *A&A*, 300, 823
- Liu F.K., & Wu X.-B., 2002, *A&A*, 388, L48
- Liu F.K., Wu X.-B., Cao S.L., 2003, *MNRAS*, 340, 411
- Liu F.K., Xie G.Z., Bai J.M., 1995a, *A&A*, 295, 1
- Lobanov A.P., Roland J., 2005, *A&A*, 431, 831
- Lomb N.R., 1976, *Ap&SS*, 39, 447
- Lu J.-F., Lin Y.-Q., Gu W.-M., 2004, *ApJ*, 602, L37

- McLure R.J., & Dunlop J.S. 2004, MNRAS, 352, 1390
- Merritt D., Ekers R.D., 2002, Sci, 297, 1310
- Merritt D., & Ferrarese L. 2001, ApJ, 547, 140
- Merritt D., Milosavljevic M., 2005, Liv. Rev. Relat., Vol.8, No.8
- Meyer F., Meyer-Hofmeister E. 1994, A&A, 288, 175
- Meyer F., Liu B.F., Meyer-Hofmeister E. 2000, A&A, 354, L67
- Meyer-Hofmeister E., Liu B.F., Meyer F., 2005, A&A, 432, 181
- Narayan R. 2002, in Lighthouses of the Universe, Conf. Proc., ed. M. Gilfanov, R. Sunyaev, & E. Churazov, ESO Astrophysics Symposia (Springer), 405
- Narayan R., Yi I. 1994, ApJ, 428, L13
- Narayan R., Yi I. 1995, ApJ, 452, 710
- Narayan R., Igumenshchev I.V., Abramowicz M.A., 2000, ApJ, 539, 798
- Nelson C.H., & Whittle M., 1995, ApJS, 99, 67
- Netzer H., 1990, in Active Galactic Nuclei, ed. R.D. Blandford, H. Netzer, & L. Woltjer (Berlin: Springer), p.57
- Nilsson K., Charles P.A., Pursimo T., Takalo L.O., Sillanpää A., & Teerikorpi, P. 1996, A&A, 314, 754
- Onken C.A., Ferrarese L., Merritt D., Peterson B.M., Pogge R.W., Vestergaard M., Wandel A. 2004, ApJ, 615, 645
- Ostorero L., Villata M., Raiteri C.M., 2004, A&A, 419, 913
- Peters P.C., Mathews J., 1963, Phys. Rev., 131, 435
- Peterson B.M., Ferrarese L., Gilbert K.M., Kaspi S., Malkan M.A., et al., 2004, ApJ, 613, 682
- Qian B., Tao J., 2004, PASP, 116, 161
- Raiteri C. M., Villata M., Aller H. D., Aller M.F., Heidt J., et al. 2001, A&A, 377, 396

- Raiteri C.M., Villata M., Ibrahimov M.A., Larionov V.M., Kadler M., et al. 2005, *A&A*, 438, 39
- Raiteri C.M., Villata M., Kadler M., Krichbaum T.P., Boettcher M., et al., 2006, *A&A*, 452, 845
- Rezzolla L., Yoshida S., Maccarone T.J., Zanotti O., 2003a, *MNRAS*, 344, L37
- Rezzolla L., Yoshida S., Zanotti O., 2003b, *MNRAS*, 344, 978
- Rieger F.M., 2004, *ApJ*, 615, L5
- Romero G.E., Combi J.A., Benagli P., Azcarate I.N., Cersosimo J.C., Wilkes L.M., 1997, *A&A*, 326, 77
- Roy M., Papadakis I.E., Ramos-Colón E., Sambruna R., Tsinganos K., et al. 2000, *ApJ*, 545, 758
- Róžańska A., Czerny B., 2000, *MNRAS*, 316, 473
- Rubio-Herrera E., Lee W.H., 2005a, *MNRAS*, 357, L31
- Rubio-Herrera E., Lee W.H., 2005b, *MNRAS*, 362, 789
- Scargle J.D. 1982, *ApJ*, 263, 835
- Sillanpää A., Haarala S., Valtonen M.J., Sundelius B., Byrd G.G., 1988, *ApJ*, 325, 628
- Sillanpää A., Takalo L.O., Pursimo T., Nilsson K., Heinamaki P., et al. 1996, *A&A*, 315, L13
- Smith, P. S., Balonek, T. J., Elston, R., Heckert, P. A., 1987, *ApJS*, 64, 459
- Strohmayer T.E., Zhang W., Swank J.H., et al., 1996, *ApJ*, 469, L9
- Sudou H., Iguchi S., Murata Y., Taniguchi Y., 2003, *Sci*, 300, 1263
- Teräsranta H., Achren J., Hanski M., Heikkilä J., Holopainen J., et al. 2004, *A&A*, 427, 769
- Teräsranta H., Tornikoski M., Mujunen A., Karlamaa K., Valtonen T., et al. 1998, *A&AS*, 132, 305
- Thorne K.S., Braginskii V.B., 1976, *ApJ*, 204, L1
- Török G., 2005, *A&A*, 440, 1

- Tremaine S., Gebhardt K., Bender R., Bower G., Dressler A., et al. 2002, ApJ, 574, 740
- Ulrich M.-H., Maraschi L., Urry C.M., 1997, ARA&A, 34, 445
- Urry C.M., Padovani P., 1995, PASP, 107, 803
- Valtaoja E., Teräsanta H., Tornikoski M., Sillanpää A., Aller M.F., et al, 2000, ApJ, 531, 744
- van der Klis, M., 1989, ARA&A, 27, 517
- Villata M., Raiteri C.M., Sillanpaa A., Takalo L.O., 1998, MNRAS, 293, L13
- Wagner S.J., & Witzel A., 1995, ARA&A, 33, 163
- Waltman E. B., Fiedler R.L., Johnston K.J., Spencer J.H., Florkowski D.R., et al. 1991, ApJS, 77, 379
- Wang J.-M., Luo B., Ho L.C., 2004, ApJ, 615, L9
- Webb J.R., Howard E., Benítez E. 2000, AJ, 120, 41
- Webb J.R., & Smith A.G., 1989, A&A, 220, 65
- Wu X.-B., Wang R., Kong M.Z., Liu F.K., & Han J.L. 2004, A&A, 424, 793
- Wu J.H., Zhou X., Wu X.-B., Liu F.K., Ma J., et al. 2006, AJ, in press
- Zanotti O., Rezzolla L., Font J.A., 2003, MNRAS, 341, 832
- Zhao G., Liu F.K., Wu X.-B., 2006, in preparation.
- Zheng W. 1988, ApJ, 324, 801

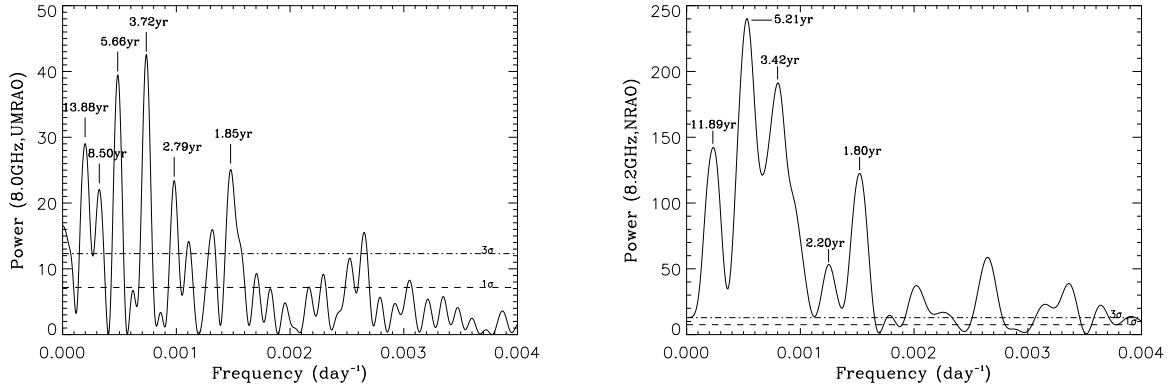


Fig. 3.— The power spectrum of the radio light curves at 8.0 GHz at UMRAO (*left*) and at 8.2 GHz at NRAO (*right*). The identified QPOs are indicated. The dashed and the dash-dotted lines are the  $1\sigma$  and  $3\sigma$  significance levels, respectively.



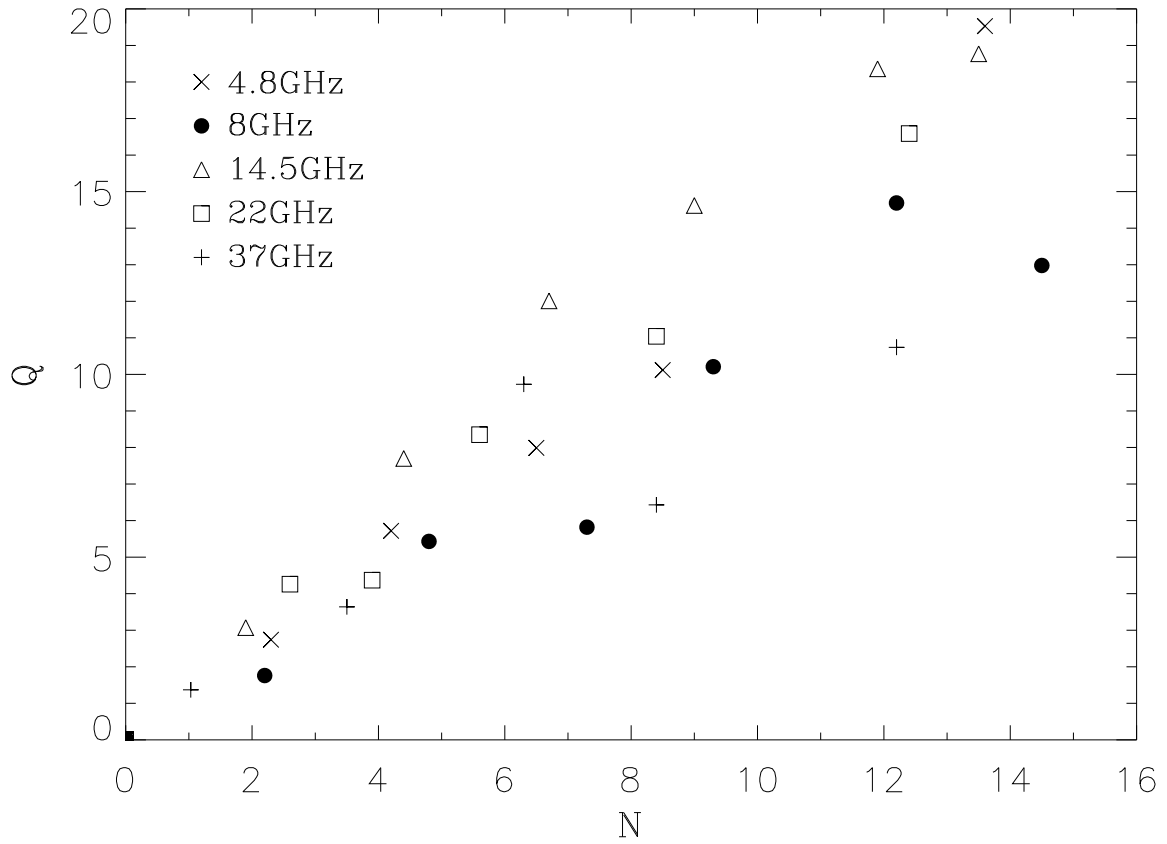


Fig. 4.— Quality factor  $Q$  vs repetition number  $N$  of QPOs in the combined radio light curves. The correlation of  $Q$  and  $N$  implies that the  $Q$ -value is limited by the monitoring time of the object and much longer observations are needed to give stringent constraint on the intrinsic coherence of QPOs.

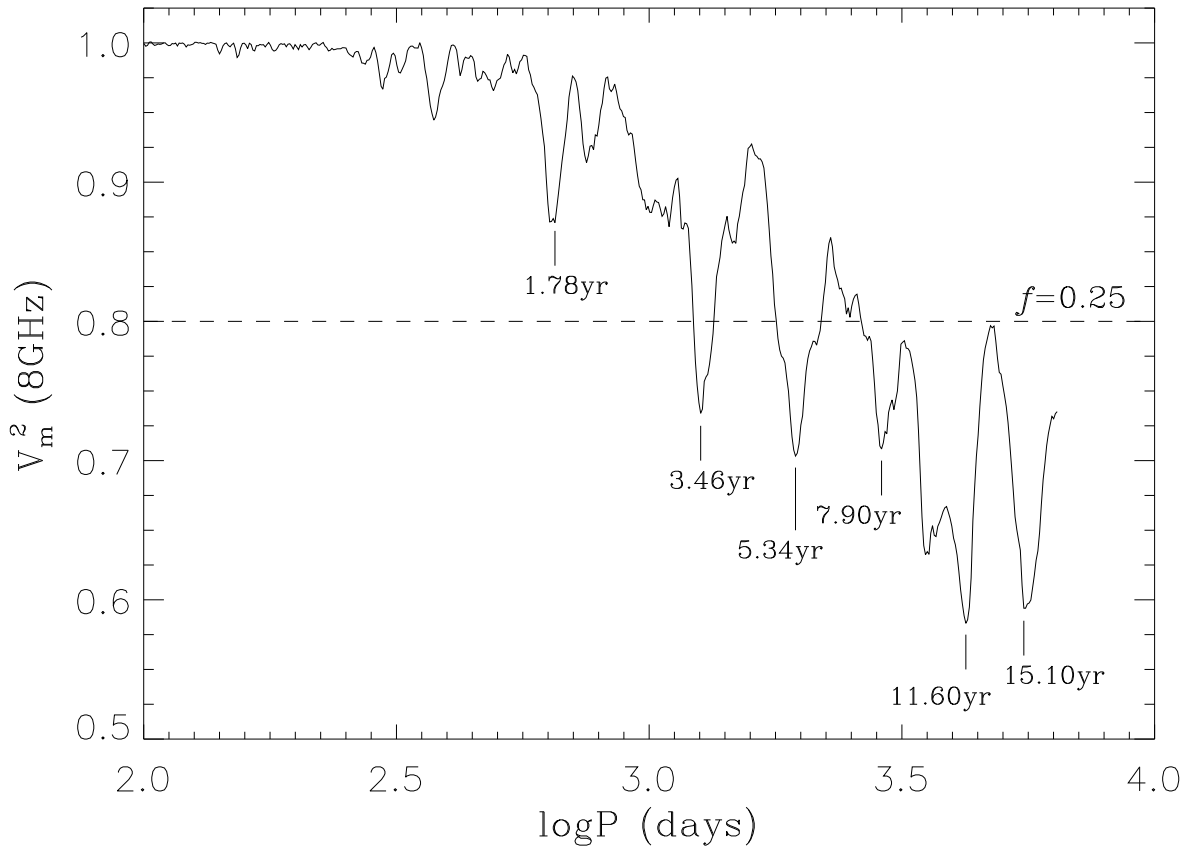


Fig. 5.— Normalized Jurkevich periodic analysis results of the combined radio light curve at 8 GHz. The minima corresponding to periods 1.78 yrs, 3.46 yrs, 5.34 yrs, 7.90 yrs and 11.60 yrs are prominent. A period is strong if  $f > 0.25$  with  $f = (1 - V_m^2)/V_m^2$

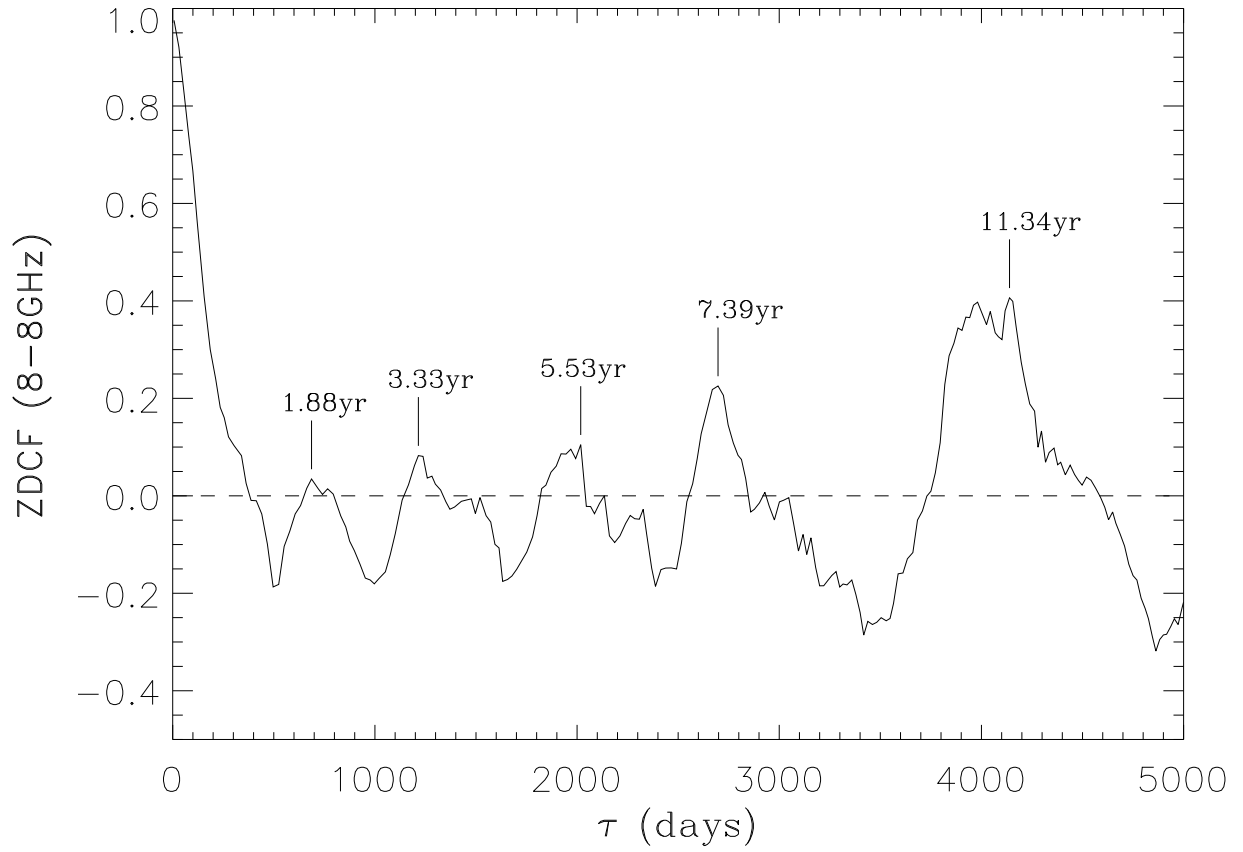


Fig. 6.— The periodic analysis results with ZDCF method. The results are consistent with that of Jurkovich  $V_m^2$  method and the two weakest QPOs at Lomb’s periodogram are missing.

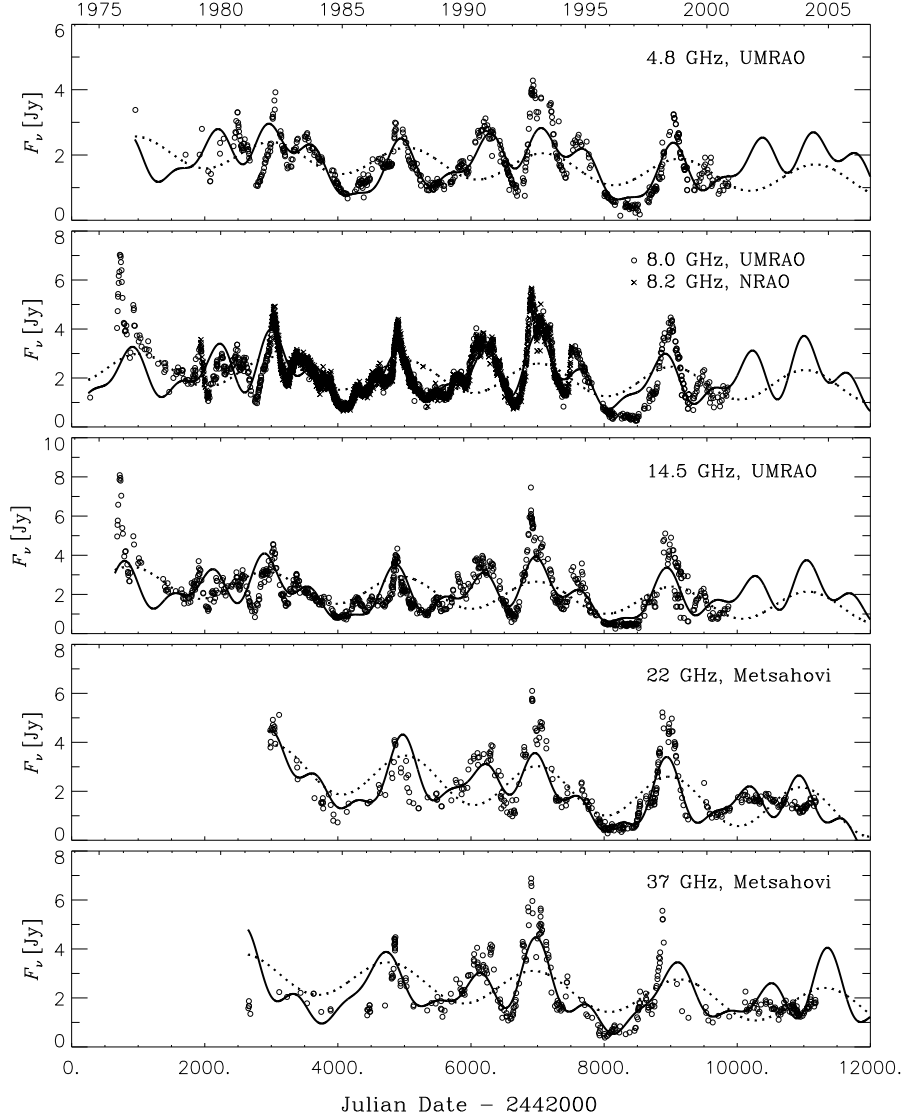


Fig. 7.— The radio light curves of AO 0235+164. The observation frequencies are indicated at the upper right corner in the figures. The solid line is the result fitted with six QPOs and the dotted line is the result fitted with the fundamental QPO of period  $P_s$ . The results clearly showed that in addition to the fundamental QPO the other five QPO harmonics significantly contributed to the variations of the radio light curves.

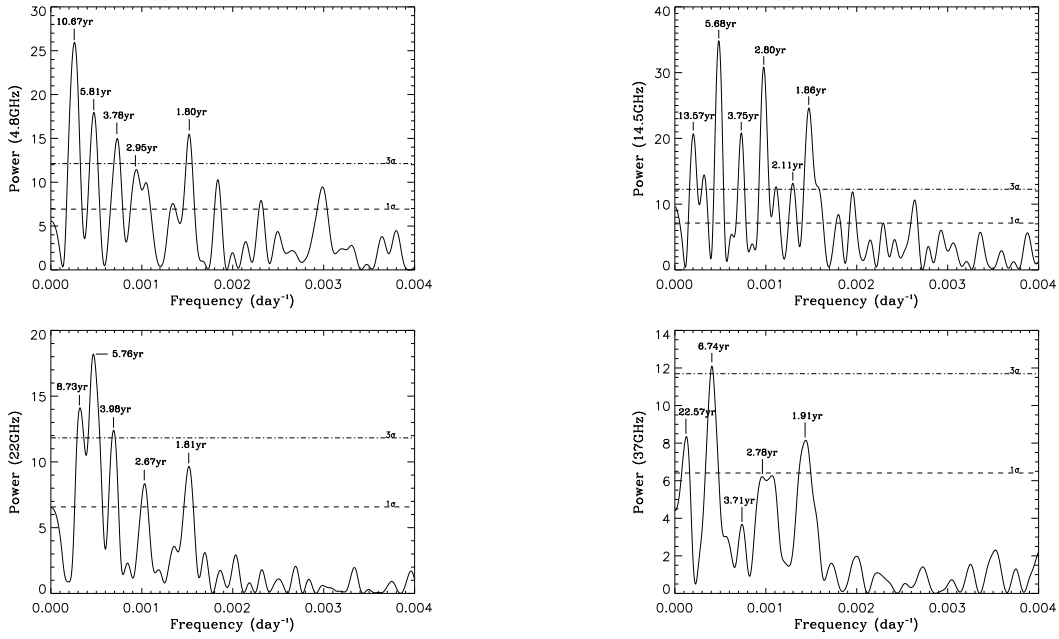


Fig. 8.— Lomb periodograms of the radio light curves at 4.8 GHz (*uper left*), 14.5 GHz (*uper right*), 22 GHz (*lower left*), and 37 GHz (*lower right*). Fitted centroid periods of QPOs with Gaussian function are indicated. The dashed and dash-dotted lines are the  $1\sigma$  and  $3\sigma$  significance levels, respectively. The radio data at 4.8 GHz and 14.5 are from UMRAO and at 22 GHz and 37 GHz from Metsähovi Observatory.

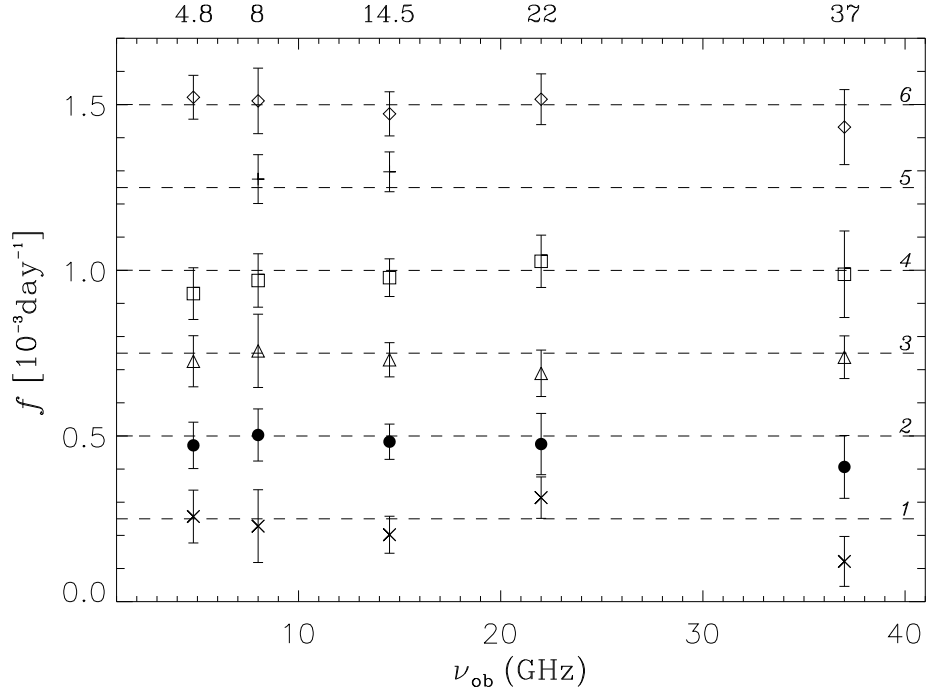


Fig. 9.— Dependence of QPO frequencies on radio frequencies. The horizontal dashed lines with small integer number  $N = 1, 2, 3, 4, 5,$  and  $6$  indicates the expected ratio of frequencies of QPOs and the basic QPO with lowest frequency (calculated basing the fundamental QPO frequency  $\nu_s$  at 8 GHz). The centroid frequencies and the harmonic relationship of QPOs are independent of the observational radio frequencies.

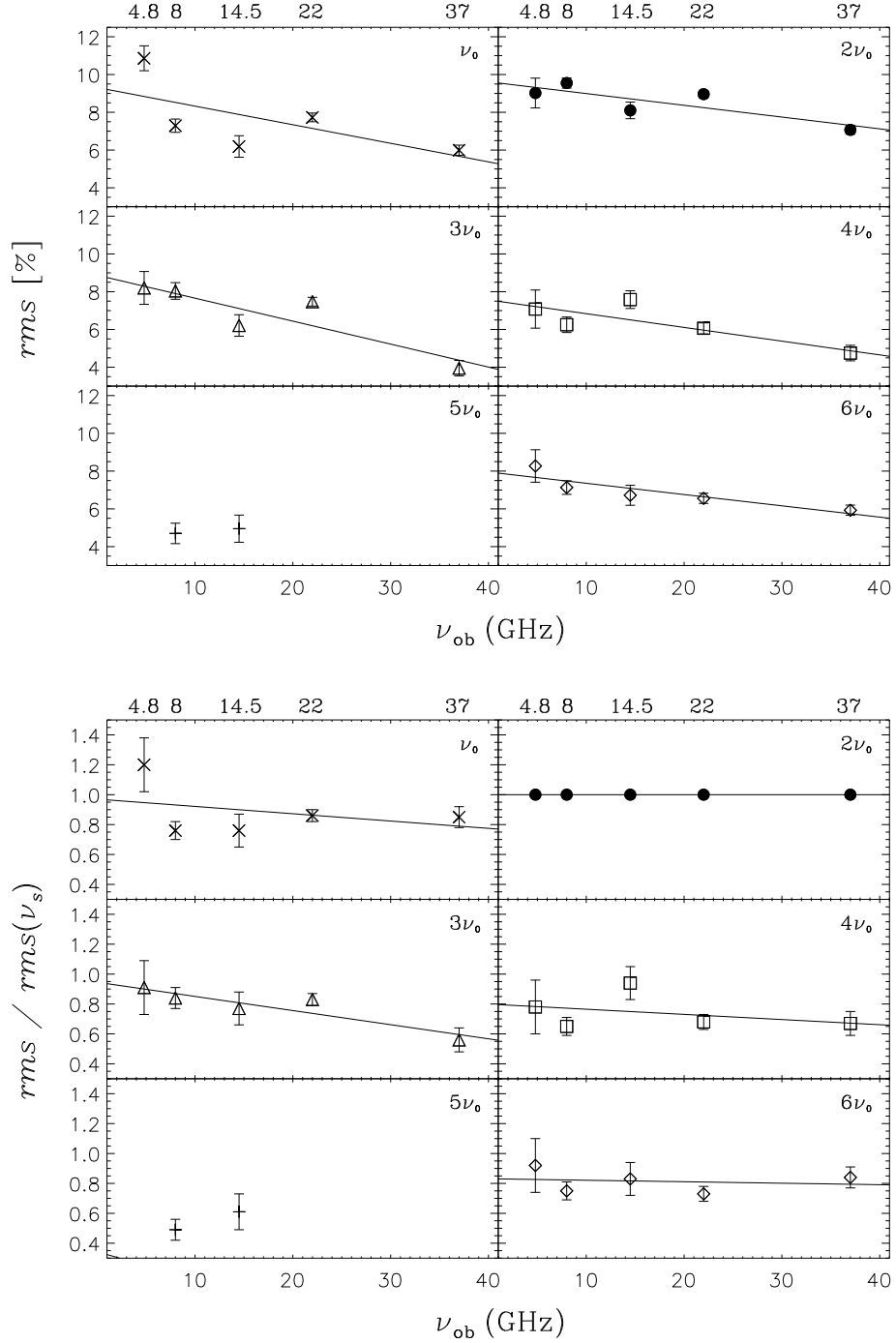


Fig. 10.— The amplitude  $rms$  (in percentage) of QPO harmonics as a function of the radio frequencies (*upper panel*) and the amplitude  $rms$  relative to that of the fundamental QPO (the 2nd harmonics) *vs* radio frequencies (*lower panel*). The solid line is the fitted results with least square method.

Table 1: Hormanic QPOs in the radio light curves at 4.8 GHz, 8 GHz, 14.5 GHz, 22 GHz and 37 GHz analyzed with the Lomb power spectrum method.

$\nu_{obs}$ $\bar{P}_s$ (yr <sup>-1</sup> )	$\nu$ (10 <sup>-3</sup> day <sup>-1</sup> )	$rms$ (%)	P (yr)	Q	$\chi^2$	N	$\nu/\nu_s$	Id.	$\Delta\phi_0$ ( $\pi$ )	
8 GHz	0.2279±0.1098	7.29±0.35	12.02±5.79	1.76	0.431	2.2	0.45	1	-0.39	
	0.5029±0.0787	9.55±0.27	5.45±0.85	5.43	0.485	4.8	1.00	2	0.00	
	5.46	0.7568±0.1105	8.04±0.44	3.62±0.53	5.82	0.485	7.3	1.50	3	-0.17
	±0.47	0.9691±0.0806	6.25±0.41	2.83±0.24	10.21	0.485	9.3	1.93	4	0.98
		1.275±0.074	4.70±0.54	2.15±0.12	14.69	0.162	12.2	2.54	5	-0.58
		1.511±0.099	7.13±0.36	1.81±0.12	12.98	0.332	14.5	3.00	6	0.07
4.8 GHz	0.2568±0.0797	10.86±0.66	10.67±3.31	2.74	0.132	2.3	0.54	1	-0.35	
	0.4716±0.0700	9.02±0.79	5.81±0.86	5.72	0.031	4.2	1.00	2	0.00	
	5.62	0.7254±0.0771	8.20±0.87	3.78±0.40	7.99	0.085	6.5	1.54	3	-0.19
	±0.44	0.9295±0.0780	7.08±1.01	2.95±0.25	10.12	0.019	8.5	1.97	4	1.19
									(5)	(-0.41)
		1.522±0.066	8.27±0.86	1.80±0.08	19.53	0.006	13.6	3.23	6	0.36
14.5 GHz	0.2019±0.0558	6.19±0.57	13.57±3.75	3.07	0.014	1.9	0.42	1	-0.34	
	0.4826±0.0532	8.10±0.44	5.68±0.63	7.70	0.251	4.4	1.00	2	0.00	
	5.53	0.7299±0.0516	6.21±0.57	3.75±0.27	12.01	0.033	6.7	1.51	3	-0.11
	±0.33	0.9776±0.0568	7.58±0.47	2.80±0.16	14.62	0.041	9.0	2.03	4	1.22
		1.297±0.060	4.95±0.72	2.11±0.10	18.36	0.002	11.9	2.69	5	-0.40
		1.472±0.067	6.72±0.53	1.86±0.08	18.77	0.004	13.5	3.05	6	0.44
22 GHz	0.3138±0.0625	7.73±0.23	8.73±1.74	4.26	0.087	2.6	0.66	1	-0.12	
	0.4755±0.0924	8.96±0.20	5.76±1.12	4.37	0.087	3.9	1.00	2	0.00	
	5.55	0.6890±0.0701	7.47±0.23	3.98±0.40	8.35	0.025	5.6	1.45	3	-0.34
	±0.47	1.027±0.079	6.06±0.29	2.67±0.21	11.04	0.015	8.4	2.16	4	0.94
									(5)	(-0.29)
		1.516±0.078	6.56±0.27	1.81±0.09	16.59	0.015	12.4	3.19	6	-0.02
37 GHz	0.1214±0.0753	5.99±0.27	22.57±14.00	1.37	0.039	1.03	0.30	1	-0.55	
	0.4065±0.0948	7.07±0.23	6.74±1.57	3.64	0.040	3.5	1.00	2	0.00	
	5.77	0.7376±0.0644	3.95±0.41	3.71±0.32	9.73	0.040	6.3	1.81	3	0.19
	±0.64	0.9879±0.1305	4.75±0.41	2.78±0.37	10.74	0.073	8.4	2.43	4	-0.42
									(5)	(0.36)
		1.432±0.113	5.93±0.27	1.91±0.15	9.13	0.073	12.2	3.52	6	-0.77